EARTH SCIENCES
RESEARCH JOURNAL
Earth Sci. Res. J. Vol. 28, No. 2 (June, 2024): 103 - 126

UNIVERSIDAD NACIONAL DE COLOMBIA

PALEONTOLOGY

A new species of *Platypterygius* (Ophthalmosauridae) from the lower Barremian of Colombia and assessment of the species composition of the genus

María E. Páramo-Fonseca[1]*, Cristian D. Benavides-Cabra[1,2], Renzo A. Garavito-Camacho[1]
1. Departamento de Geociencias, Universidad Nacional de Colombia, Bogotá, Colombia, meparamof@unal.edu.co; cdbenavidesc@unal.edu.co; rgaravitoc@unal.edu.co
2. Museo Geológico Nacional José Royo y Gómez, Servicio Geológico Colombiano, Bogotá, Colombia
* Corresponding author: meparamof@unal.edu.co

ABSTRACT

In this paper, we describe a new ophthalmosaurid specimen found in the lower Barremian beds of the Paja Formation at Villa de Leiva, Boyacá, Colombia. The specimen represents a new species of *Platypterygius*, *P. elsuntuoso* sp. nov. defined by three unique features within the genus: a small ventral peg in the anterior ventral border of the extracondylar area of the basioccipital; a supratemporal groove in the quadrate; and a shallow neck at the base of the acellular cementum ring on the teeth root. In support of our taxonomic determination, in this contribution we also assess the species composition of the genus *Platypterygius*, comparing the known anatomy of the type species *P. platydactylus* with that of the other species previously assigned to the genus. We found that a great morphological affinity in the forelimb of the species *P. americanus*, *P. australis*, *P. hercynicus*, and *P. sachicarum* (lower Barremian to lower Cenomanian) with that of the type species (Aptian) is unquestionable and differentiate them from all other ophthalmosaurids. Three new diagnostic features (synapomorphies of the genus) support their inclusion in *Platypterygius*. Consequently, the genus name "*Kyhytysuka*", recently proposed to differentiate *P. sachicarum* from the genus *Platypterygius* is here rejected. A careful comparison of the cranial characteristics of *Platypterygius* specimens preserving associated cranial and fin remains demonstrate that *Platypterygius* is a genus distinguishable from other ophthalmosaurids not only by a typical forelimb but also by a particular combination of skull features. In this context, the skull morphology of "*Simbirskiasaurus*" concurs with that defining *Platypterygius* and its minor differences are not sufficient to support its generic distinction. The morphological comparisons and our phylogenetic analysis show the new species *P. elsuntuoso* more closely related to the Colombian species *P. sachicarum* than to other species of *Platypterygius*. Given that the new species came from the lower Barremian and *P. sachicarum* came from the upper Barremian, the minor differences in dentition found between the two species suggest a speciation by adaptation to new food sources in the Cretaceous epicontinental sea of Colombia.

Keywords: Ophthalmosauridae; Platypterygius; Barremian; Colombia

Una nueva especie de *Platypterygius* (Ophthalmosauridae) del Barremiano inferior de Colombia y evaluación de la composición específica del género

RESUMEN

En este artículo describimos un nuevo espécimen de ofthalmosáuridos encontrado en capas de la Formación Paja, en Villa de Leiva, Boyacá, Colombia. El espécimen representa una nueva especie del género *Platypterygius*, *P. elsuntuoso* sp. nov., definida por tres características únicas dentro del genero: un pequeño proceso en el borde anterior ventral del área extracondilar del basioccipital; una hendidura supratemporal en el cuadrado; y un ligero cuello en la base del anillo de cemento acelular de las raíces de los dientes. Como soporte a nuestra determinación, en esta contribución también evaluamos la composición específica del género *Platypterygius*, comparando la anatomía conocida de la especie tipo *P. platydactylus* con la de las demás especies previamente asignadas al género. Encontramos que hay una incuestionable afinidad morfológica entre la aleta anterior de las especies *P. americanus*, *P. australis*, *P. hercynicus*, y *P. sachicarum* (Barremiano inferior al Cenomaniano inferior) y la de la especie tipo (Aptiano), que las diferencia de todos los demás oftalmosáuridos. Tres nuevos caracteres diagnósticos (sinapomorfías para el género) soportan su inclusión en *Platypterygius*. Consecuentemente, el nombre genérico "*Kyhytysuka*", recientemente propuesto para diferenciar *P. sachicarum* del género *Platypterygius*, es aquí descartado. Una comparación cuidadosa de las características craneales de los especímenes de *Platypterygius* que preservan la aleta anterior asociada demuestra que *Platypterygius* es un género que se distingue de otros oftalmosáuridos no sólo por su aleta anterior típica, sino también por una combinación particular de rasgos craneanos. En este contexto, la morfología del cráneo de "*Simbirskiasaurus*" coincide con la definida para *Platypterygius*, y sus pocas diferencias no son suficientes para soportar una distinción genérica. Las comparaciones morfológicas y nuestro análisis filogenético muestran a la especie nueva, *P. elsuntuoso*, está más cercanamente relacionada con la especie colombiana *P. sachicarum* que con las demás especies de *Platypterygius*. Dado que la nueva especie proviene del Barremiano inferior y *P. sachicarum* del Barremiano superior, las diferencias menores que encontramos entre sus denticiones sugieren un proceso de especiación por adaptación a nuevas fuentes de alimento en el mar epicontinental Cretácico de Colombia.

Palabras clave: Ophthalmosauridae; Platypterygius; Barremiano; Colombia

Record
Manuscript received: 02/01/2024
Accepted for publication: 09/07/2024

How to cite this article:
Páramo-Fonseca, M. E., Benavides-Cabra, C. D., & Garavito-Camacho, R. A. (2024). A new species of Platypterygius (Ophthalmosauridae) from the lower Barremian of Colombia and assessment of the species composition of the genus. *Earth Sciences Research Journal, 28*(2), 103-126. https://doi.org/10.15446/esrj.v28n2.112332

ISSN 1794-6190 e-ISSN 2339-3459
https://doi.org/10.15446/esrj.v28n2.112332

1. Introduction

The Barremian-Aptian beds of the Arcillolitas abigarradas Member of the Paja Formation are known for preserving abundant specimens of marine reptiles in the Villa de Leiva-Sáchica-Sutamarchán region (Cadena, 2015; Cadena et al., 2019; Cadena & Parham, 2015; Cortés et al., 2019; Cortés & Páramo-Fonseca, 2018; Gómez-Pérez & Noè, 2017; Maxwell et al., 2016; 2019; Páramo-Fonseca, 2015; Páramo-Fonseca et al., 2016; 2018; 2019a; 2019b; 2021). Numerous ichthyosaur specimens have been found in this region, most of which are currently under study. Two ophthalmosaurid taxa have been described so far: *Platypterygius sachicarum* Páramo, 1997, recently placed under "*Kyhytysuka*" *sachicarum* by Cortés et al. (2021) and known from two specimens collected from upper Barremian beds (Benavides-Cabra et al., 2023; Maxwell et al., 2019; Páramo, 1997) and *Muiscasaurus catheti* Maxwell et al., 2016, known from two specimens collected from upper Aptian beds (Benavides-Cabra et al., 2023; Maxwell et al., 2016; Páramo-Fonseca et al., 2021). A new ophthalmosaurid specimen from the lower Barremian showing great affinities with the *Platypterygius* Huene, 1922 morphology is here described. It consists of an almost complete skull, disarticulated axial remains and scarce appendicular elements.

The name *Platypterygius* was coined by Huene (1922) to receive *Ichthyosaurus platydactylus* (Broili, 1907), known from a single specimen. However, the type specimen of *Platypterygius platydactylus* was lost in World War II (Kolb & Sander, 2009) and the only available information from the holotype consists of the description and drawings of Broili (1907). After the revision of Cretaceous ichthyosaurs by McGowan (1972), *Platypterygius* became the sole genus identified from Cretaceous rocks, creating the impression of low ichthyosaur diversity during the Cretaceous (Fischer et al., 2014a). Recently, the study of new material and the review of Cretaceous ichthyosaur collections have led to reevaluate this low diversity (Druckenmiller & Maxwell, 2010; Fischer, 2012; 2016; Fischer et al., 2011; 2012; 2014a; 2014b; 2014c; 2016; Maxwell et al., 2016; 2019; Maxwell & Caldwell, 2006a; 2006b; Páramo-Fonseca et al., 2021) and have also led some authors to contest the stability and taxonomic validity of the genus *Platypterygius* (Fischer, 2012; 2016; Fischer et al., 2014a; 2014c; 2016; Ji et al., 2016; Maxwell et al., 2019; Moon, 2019; Zammit, 2011).

In this context, the taxonomic placement of the new specimen here described required a revision of the morphology of the species included in the genus *Platypterygius*. As a result, in this contribution we add our assessment of the species composition of the genus and its diagnostic features.

2. Geographic and geological context

The specimen here described was found in an *ex-situ* concretion in La Cabrera hill, northwest of Villa de Leiva (Boyacá, Colombia) where the Arcillolitas abigarradas Member of the Paja Formation outcrops (Fig. 1A, B). Its exact geographic provenance is unknown, so it was not possible to determine its precise stratigraphic position. However, numerous ammonoid specimens were extracted from the same concretion and some of them have been preliminarily identified as *Acanthoptychoceras sp.* Manolov, 1962 (Benavides-Cabra et al., 2023) (Fig. 1C). Following the Barremian ammonite zonation proposed by Patarroyo (2000; 2004), this genus is included in the *Nicklesia pulchella* biozone, which according to this author represents the lower Barremian in Colombia.

The Paja Formation was described in the Villa de Leiva-Sáchica-Sutamarchán region by Etayo-Serna (1968a). It is a predominantly argillaceous unit, from which this author recognized three different lithostratigraphic units, which he named from base to top: Arcillolitas negras, Arcillolitas abigarradas and Arcillolitas con nódulos huecos. The new ichthyosaur specimen most likely comes from the middle unit, the Arcillolitas abigarradas Member, which according to Etayo-Serna (1968a) represents the Barremian-Aptian in the Villa de Leiva - Sáchica - Sutamarchán region. This Member is composed of gypsum-rich, variegated mudstones containing abundant calcareous concretions, interbedded with thin calcareous, marly, and sandy levels (Etayo-Serna, 1965; 1968a). Based on the ammonoids associated with the specimen here described, we estimated the stratigraphic origin of the ichthyosaur specimen from the lower part of the Arcillolitas abigarradas Member of the Paja Formation (sensu Etayo-Serna, 1965; 1968a; 1979) (Fig. 1B), more precisely from the segment "A" or "B" of Etayo-Serna (1968a; 1979) or segment "I" of Forero and Sarmiento (1985). The lithologic succession of the Arcillolitas abigarradas Member has been interpreted as tidal plain salt deposits in an environment protected from the influence of the open sea (Forero & Sarmiento, 1985). This Member is a rich fossiliferous unit containing abundant ammonoids (Etayo-Serna, 1965; 1968a; 1968b; 1979; Hoedemaeker, 2004; Patarroyo, 2000; 2004; 2009; 2020) and well-preserved remains of plants, bivalves, fish, marine reptiles and dinosaurs (Cadena, 2015; Cadena et al., 2019; Cadena & Parham, 2015; Carballido et al., 2015; Carrillo-Briceño et al., 2019; Cortés et al., 2019; 2021; Cortés & Páramo-Fonseca, 2018; Gómez-Pérez & Noè, 2017; Huertas, 1970; Maxwell et al., 2016; 2019; Noè & Gómez-Pérez, 2022; Noè & Gómez–Pérez, 2020; Páramo-Fonseca, 2015; Páramo-Fonseca et al., 2016; 2018; 2019a; 2019b; 2021; Schultze & Stöhr, 1996; van Waveren et al., 2002).

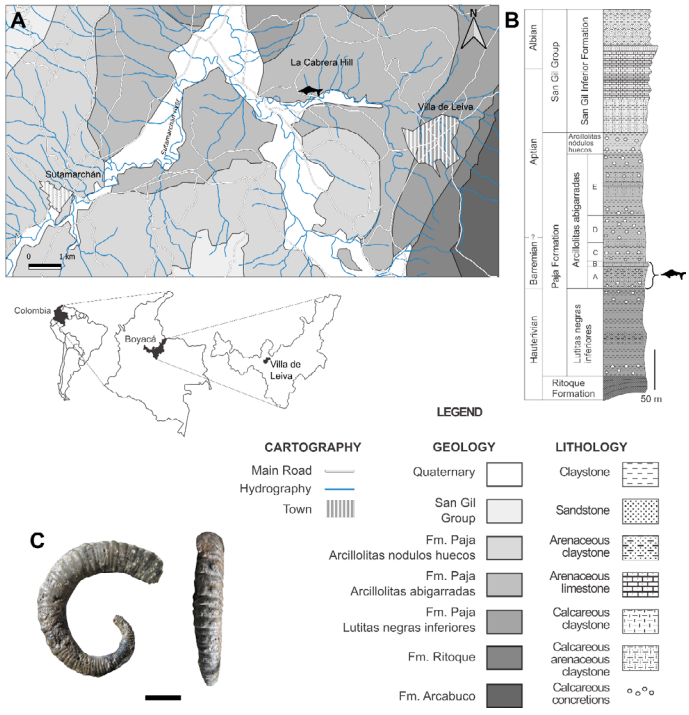

Figure 1. Geographic and stratigraphic provenance of the specimen FCG-CBP-28. **A**, Geological map showing the finding site (ichthyosaur silhouette) (modified from Etayo-Serna, 1968a). Cartographic base: Instituto Geográfico Agustín Codazzi. **B**, generalized stratigraphic section of the Paja Formation cropping out around Villa de Leiva - Sáchica - Sutamarchán region, showing the stratigraphic origin of the specimen (ichthyosaur silhouette) (modified from Etayo-Serna, 1979). **C**, Lateral and ventral views of the ammonoid *Acanthoptychoceras* sp. extracted from the concretion bearing the ichthyosaur specimen. Scale bar = 10 mm.

3. Materials and methods

The new specimen (FCG-CBP-28) was collected in 1999 by the Fundación Colombiana de Geobiología (FCG). It is currently housed in the collection of the Centro de Investigaciones Paleontologicas (CIP). The fossil was extracted in six fragments forming a large concretion. It was prepared by M. L. Parra-Ruge and J. D. Parra-Ruge, from the Fundación Colombiana de Geobiología and Centro de Investigaciones Paleontológicas (CIP) during 2000-2007, and recently, some preparation details were done by F. Parra-Ruge from the CIP. The preparation was done through mechanical and chemical methods following the techniques developed by the FCG (Padilla et al., 2010).

The specimen consists of a skull, some axial elements including the atlas-axis and a few cervical vertebrae, the left coracoid, and a few phalanges. The bones of the right side of the skull are well-preserved, contrasting from the bones of the left side of the skull and those of the occipital region, which are displaced from their original position. Thus, the description of the skull is primarily based on its right side. The descriptive drawings were based on photographs and direct observations on the fossil and the final figures were made with the open-source software Inkscape 1.2. The areas of the sclerotic ring and the orbit were calculated on photographs using the measurement tools included in the Inkscape software and were then used to estimate the ontogenetic stage of the individual (following Fernández et al., 2005). A 3D photogrammetric model of

the basioccipital is provided supporting the anatomical description of the specimen (see Supplemental Data 1). The model was produced by H. D. Palma-Castro from Departamento de Biología of the Universidad Nacional de Colombia. It was obtained from raw 18 megapixels (5184 x 3456 px) images using high-resolution structure from motion techniques. The basioccipital was photographed with a Canon EOS rebel 4000D camera and processed using 779 pictures. Photos were taken surrounding the basioccipital at two different angles to ensure the maximum possible resolution and coverage. The model has been scaled using two scale bars located in each image. The software Agisoft Metashape Professional 1.5.1, Meshlab v2022.02, and Blender 3.3.1 were used to obtain the 3D model.

We conducted the morphological comparisons of the new specimen with the Cretaceous and Late Jurassic ophthalmosaurids, as well as the assessment of the genus *Platypterygius*, based on published descriptions and direct observations on the Colombian material. We performed a phylogenetic analysis to determine the position of the new specimen within Ophthalmosauridae. We based our analysis on the updated dataset of Barrientos-Lara and Alvarado-Ortega (2021b), which itself is a modified version of the dataset published by Barrientos-Lara and Alvarado-Ortega (2020). We scored *M. catheti* (CIP-FCG-CBP-74; FCG-CBP-16) and *P. sachicarum* (DON-19671) based on the scoring provided in Páramo-Fonseca et al. (2021) and on personal observations. We scored the specimen CIP-GA-01042014, referred by Maxwell et al. (2019) to *P. sachicarum*, and the specimen FCG-CBP-87 referred by Cortés & Páramo-Fonseca (2018) to *Platypterygius* sp., based on the authors' description and personal observations. Furthermore, we added the following OTUs: *Jabalisaurus meztli* Barrientos-Lara & Alvarado Ortega, 2021a based on the scoring of Barrientos-Lara & Alvarado-Ortega (2021a); *Pervushovisaurus bannonvkensis* Arkhangelsky, 1998, based on the scoring and description of Fischer et al. (2014c); *Plutoniosaurus bedengensis* Efimov, 1997 based on the scoring provided by Zverkov & Jacobs (2020) and on the publication of Efimov (1997); *Thalassodraco etchesi* Jacobs & Martill, 2020 based on the scoring and description provided by Jacobs & Martill (2020); *Sumpalla argentina* Campos et al. 2021, based on the scoring and description provided by Campos et al. (2021); and *Catutosaurus gaspariniae* Fernández et al., 2021 based on the scoring and description provided by Fernández et al. (2021). Additionally, we modified the scoring of *Ophthalmosaurus* Seeley, 1874 based on the scoring revision of Páramo-Fonseca et al. (2021). We also revised the scoring of *P. americanus* (Nace, 1939), *P. platydactylus*, *P. hercynicus* Kuhn, 1946, *P. australis* (M'Coy, 1867), and "*Simbirskiasaurus*" *birjukovi* Ochev & Efimov, 1985 based on the published descriptions of these taxa (Broli, 1907; Fischer, 2012; Fischer et al. 2014c; Kear, 2005; Kolb & Sander, 2009; Kuhn, 1946; Maxwell & Kear, 2010; Romer, 1968; Wade, 1984; 1990; Zammit et al., 2010). For the Upper Jurassic Boreal Realm ichthyosaurians we used the names proposed by Zverkov & Efimov (2019) and Zverkov and Prilepskaya (2019).

We modified one character, removed two and added two new characters to this dataset (see Supplemental Data 2). The scoring of these new characters was based on the published descriptions and illustrations of the OTUs involved in the analysis (see Supplemental Data 2: Table S1-S2). The new data matrix was compiled using the Mesquite software 3.51 (Maddison & Maddison, 2018) (see Supplemental Data 3).

The cladistic analysis was run with 52 (OTUs) and 145 characters, using TNT (v1.6) (Goloboff & Morales, 2023). All characters were treated as unordered and were equally weighted. An initial exploration for the shortest-length tree islands was performed using the new technology search options (Ratchet + Drift + Tree fusing) with 200 ratchet iterations (1 random seed) and a 99,999 trees limit. The resulting trees were then used as the starting point for a Tree bisection and reconnection (TBR) branch swapping algorithm. A strict consensus was obtained and the iterPCR algorithm was applied to identify unstable OTUs (Pol & Escapa, 2009). The Retention (RI) and Consistency (CI) indexes (Farris, 1989) were calculated, and Bremer Support values (Bremer, 1994) were computed for the nodes in the consensus tree using the TNT tools. Finally, the resulting strict reduced consensus tree was time calibrated using the timePaleoPhy function of the package paleotree 3.4.5 (Bapst, 2012) in R 4.2.3 (R Core Team, 2022), implementing mbl calibration with a minimum branch length of 1 Ma, and plotted using the geoscalePhylo function from the R package strap 1.6-0 (Bell & Lloyd, 2015).

Institutional abbreviations: **CIP**, Centro de Investigaciones Paleontológicas, Villa de Leiva, Colombia; **QM**, Queensland Museum; **SMSS**, Stadtisches Museum Schloss Salder, Salzgitter, Germany; **UW**, University of Wyoming, Laramie, Wyoming, USA.

The genus Platypterygius

The name *Platypterygius* was created by Huene (1922) to distinguish the Cretaceous longipinnate species, *Ichthyosaurus platydactylus*, from the Cretaceous latipinnate species, which he grouped within the genus *Myopterygius* Huene, 1922. Huene (1922) defined *Platypterygius* as an ichthyosaur with a large skull having a short postorbital region, long body, short tail anterior to the vertebral inflexion, short caudal fin, bifurcated ribs, humerus with two distal facets, longipinnate forelimb with great enlargement of the paddle by the presence of sesamoids in both edges of the paddle, and hind fin apparently not so small compared to the forelimb, as in other derived ichthyosaur genera. The type species *P. platydactylus* was described by Broili (1907) as *Ichthyosaurus platydactylus* based on an Aptian specimen from Germany. The type specimen, a near complete skeleton with crushed skull and a well-preserved forelimb, was lost during World War II (Kolb & Sander, 2009), but a description and illustration were published by Broili (1907). Both the generic and specific epithets of the type species *P. platydactylus,* emphasize the enlargement of the forelimb by hyperdactyly (Broili, 1907; Huene, 1922).

The forelimb morphology of the type species was the base for subsequent assignment of other species to the genus *Platypterygius*. Kuhn (1946) proposed and described *P. hercynicus* based on a skeleton including cranial and appendicular remains collected from the Aptian of Germany. McGowan (1972), comparing cranial and postcranial remains, in addition to the type species and *P. hercynicus* assigned to *Platypterygius* the following species: *Ichthyosaurus campylodon* Carter, 1846 from the Cenomanian of England (Carter, 1846; Fischer, 2016), *Ichthyosaurus australis* from the Albian of Australia (Jack & Etheridge, 1892; Kear, 2005; Longman, 1922; M'Coy, 1867; Wade, 1984; 1990), *Myopterygius americanus* from the Albian and lower Cenomanian of North America (Maxwell & Kear, 2010; Nace, 1939; Romer, 1968), *Myopterygius kiprijanoffi* Romer, 1968 from the Lower Cretaceous of Russia (Kiprijanoff, 1881), and *Myobradypterygius hauthali* Huene, 1927 from the Barremian of Argentina (Fernández & Aguirre-Urreta, 2005; Huene, 1927). Later, Arkhangelsky et al. (2008) erected *Platypterygius ochevi* Arkhangelsky et al. 2008 based on a nearly complete forelimb and fragmentary cranial and postcranial remains from the Albian-Cenomanian of Russia.

Cranial remains without preserved forelimb were subsequently assigned to this genus. Maisch & Matzke (2000) assigned to *Platypterygius* the species "*Simbirskiasaurus*" *birjukovi* and *Pervushovisaurus bannovkensis*, both known from cranial remains from the Cretaceous of Russia. Páramo (1997) defined *P. sachicarum* from a skull found in the upper Barremian of Colombia (Benavides-Cabra et al., 2023; Páramo, 1997).

In revision works of Ichthyosauria Maisch & Matzke (2000) synonymized *Longirostria* Arkhangelsky, 1998, *Tenuirostria* Arkhangelsky, 1998, and *Plutoniosaurus* Efimov, 1997 under *Platypterygius*, and McGowan & Motani (2003) placed *P. hercynicus* under *P. platydactylus* and *P. kiprijanoffi* as *nomina dubia*. Later, *P. hercynicus* was revalidated (Fischer, 2012; Kolb & Sander, 2009), *P. birjukovi* was reassigned to "*Simbirskiasaurus*" *birjukovi* (Fischer et al., 2014c), *P. campylodon* was assigned to *Pervushovisaurus campylodon* (Fischer, 2016), *P. ochevi* was synonymized under *Maiaspondylus cantabrigiensis* (Lydekker, 1888; Zverkov & Grigoriev, 2020), and *P. sachicarum* was assigned to a new genus "*Kyhytysuka*" (Cortés et al., 2021). Zverkov & Efimov (2019) used *Plutoniosaurus bedengensis* as a valid taxon and provided a scoring in their phylogenetic analysis. However, no detailed description or illustrations of this taxon have been published to date.

Here we review the definition of the genus *Platypterygius* based on the information available on the morphology of the type species and species assigned to it. From such a revision, we discuss and show that "*S.*" *birjukovi* and "*K.*" *sachicarum* concur with the definition of *Platypterygius*, whereas "*P.*" *hauthali* does not.

The forelimb of Platypterygius

The forelimb morphology of the type species of *Platypterygius*, *P. platydactylus*, is crucial in the definition of the genus. In fact, some characters from the forelimb that Broili (1907) employed to define the type species

(humerus widened proximally and distally with a strong trochanteric ridge, proximal carpal row in addition to radiale, intermedium and ulnare with radial and ulnar sesamoids, and fin remarkably broadened by hyperdactyly) have been subsequently considered diagnostic for the genus *Platypterygius* (Bardet, 1989; Huene, 1922; Kolb & Sander, 2009; Maisch & Matzke, 2000; McGowan, 1972; McGowan & Motani, 2003; Wade, 1984). Some other characters of the forelimb of the type species have also been reiteratively included in the published diagnoses of *Platypterygius*: intermedium not contacting the humerus (Bardet, 1989; Kolb & Sander, 2009; McGowan, 1972; McGowan & Motani, 2003); digital count not less than 7 (Bardet, 1989; Kolb & Sander, 2009; McGowan, 1972; McGowan & Motani, 2003); and phalanges thick, characteristically rectangular and closely fitting, except in the distal fin tip (Bardet, 1989; Kolb & Sander, 2009; Maisch & Matzke, 2000; McGowan, 1972; McGowan & Motani, 2003).

In the type species, *P. platydactylus*, the forelimb is tridactyl (three primary digits) (Bardet, 1989; McGowan, 1972); the intermedium is roughly pentagonal with a pointed proximal edge fitting between the radius and ulna, almost parallel anterior and posterior sides contacting radiale and ulnare, and longer distal side that articulates almost exclusively with a single distal carpal (distal carpal 3); the radiale and ulnare articulate mainly with a single distal carpal distally; and the arrangement between the proximal and distal carpals in the 2, 3 and 4 digits is in a near straight line (see Fig. 2A and Broili, 1907). The described carpal structure is also present in *P. americanus*, (Maxwell & Kear, 2010; McGowan, 1972; Nace, 1939), *P. australis* (Wade, 1984; Zammit et al., 2010), *P. hercynicus* (Kolb & Sander, 2009; Kuhn, 1946) and in two Colombian specimens preserving forelimb remains (FCG-CBP-87 and CIP-GA-01042014) recently described and assigned to *Platypterygius* sp. and *P. sachicarum* respectively (Cortés & Páramo-Fonseca, 2018; Maxwell et al., 2019). No other ophthalmosaurid for which the carpal region has been described shows this carpal structure (see Fig. 2).

Differing from the above described *Platypterygius* carpal morphology, a rhomboidal or hexagonal intermedium articulating with two distal carpals is found in *Malawania* Fischer et al., 2013, *Sumpalla*, *Catutosaurus*, *Sveltonectes* Fischer et al., 2011, *Ophthalmosaurus*, and "*P.*" *hauthali* (Fig. 2S-X) (for references see Fig. 2); an intermedium contacting the humerus is found in *Otschevia* Efimov, 1998 spp., *Brachypterygius* Huene, 1922, *Parrassaurus* Barrientos-Lara & Alvarado-Ortega, 2021b, and *Aegirosaurus* Bardet & Fernández, 2000 (Fig. 2Y-F') (for references see Fig. 2); and an intermedium with a larger facet for the distal carpal 2 or 4 is found in *Undorosaurus* Efimov, 1999 (Fig. 2G-I) and *Maiaspondylus* Maxwell & Caldwell, 2006a spp. (Fig. 2K-M) (for references see Fig. 2).

Moreover, the forelimb of *P. platydactylus*, *P. hercynicus*, *P. australis*, *P. americanus* and *P. sachicarum* shares the following combination of characters not found in other ophthalmosaurids (for comparisons and references see Figure 2): the articular facets for the ulna and the radius on the humerus are distally oriented, almost in the same plane, with an angle between them of near 170° (also found in *Gengasaurus* Paparella et al., 2016 and "*P.*" *hauthali*); the humeral facet for the ulna is slightly longer than that for the radius (Kolb & Sander, 2009; McGowan & Motani, 2003) (also found in *Parrassaurus*, *Arthropterygius lundi* Roberts et al., 2014; and *Aegirosaurus*); the facets for extrazeugopodial elements in the humerus are small, sometimes hardly noticeable (also found in *Brachypterygius*); the digital count is not less than 7 (also in *Maiaspondylus lindoei* and *Caypullisaurus* Fernández, 1997*;* and *Plutoniosaurus* see Efimov, 1997); and the forelimb phalanges are rectangular and closely fitting (also in *Sveltonectes*, *Caypullisaurus Maiaspondylus* spp. and *Aegirosaurus*) (for references see Figure 2).

"*P.*" *hauthali,* is only known almost exclusively by anterior appendicular elements. Recently, Campos et al., 2024 reviewed the holotype and referred material of "*P.*" *hauthali* and revalidated the genus *Myobradypterygius* Huene, 1927 for the reception of the materials previously assigned to "*P.*" *hauthali.*

In summary, the great morphological affinity of the forelimb of the lower Barremian to lower Cenomanian species *P. americanus*, *P. australis, P. hercynicus* and *P. sachicarum* with that of the type species *P. platydactylus,* is unquestionable. This morphology differentiates these species from all other ophthalmosaurids, supporting their inclusion in the genus *Platypterygius*. Minor variations in the size of the humeral facets for extrazeugodial elements and in the size or morphology of the zeugopodial, carpal, and distal carpal elements, support the distinction of different species within the genus (Broili, 1907; McGowan, 1972, Zammit et al., 2010, Kolb & Sander, 2009; Maxwell et al., 2019) (Fig. 2A-F).

The skull of Platypterygius

As discussed above, all Cretaceous ophthalmosaurids differ from *Platypterygius* by their forelimb morphology. Nevertheless, no forelimb remains are known in some specimens assigned to *Platypterygius* and in four others Cretaceous ophthalmosaurids: *Athabascasaurus* Druckenmiller & Maxwell, 2010, *Muiscasaurus*, "*Simbirskiasaurus*" and *Leninia* Fischer et al. 2013 (Druckenmiller & Maxwell, 2010; Fischer et al., 2013; Maxwell et al., 2016; Ochev & Efimov, 1985; Páramo-Fonseca et al., 2021). With the aim to establish morphological criteria for the identification of cranial remains not associated with forelimbs, a comparison of the cranial morphology of the species having a typical *Platypterygius* forelimb with that from other Cretaceous ophthalmosaurids is here discussed.

Specimens preserving associated skull and forelimb remains are known for the five species showing the *Platypterygius* type forelimb (*P. platydactylus, P. americanus*, *P. australis, P. hercynicus,* and *P. sachicarum*). In the description of the type specimen of *P. platydactylus* from the Aptian of Germany, Broili (1907) described the partially preserved skull, detailing the morphology of the quadrate, basioccipital, basisphenoid, stapes, articular, and teeth. Skull remains of the type specimen of *P. hercynicus* from the Aptian of Germany, named the "SGS" specimen (Salzgitter specimen) by Kolb & Sander (2009) have been preserved with the forelimbs associated (Kolb & Sander, 2009; Kuhn, 1946). These remains include premaxilla, nasal, frontal, parietal, supratemporal, jugal, sclerotic plates, quadrate, basioccipital, basisphenoid, supraoccipital, exoccipital, opisthotic and teeth (Kolb & Sander, 2009; Kuhn, 1946). The specimen UW 2421, a nearly complete skeleton from the upper Aptian of North America referred to *P. americanus*, preserves forelimb remains and the complete skull (Maxwell & Kear, 2010; McGowan, 1972; Romer, 1968). This skull was described by Romer in 1968, and no preparation or detailed descriptions have been accomplished later. Two specimens (QM F2453 and F3348) from the mid-upper Albian of Australia, preserving associated skull and forelimb remains, are reported by McGowan (1972) and recognized as *P. australis* by Wade (Wade, 1984; 1990 (as *P. longmani*)) and Zammit et al. (2010). The specimen QM F2453 preserves the complete skull, but no detailed description of this skull has yet been published. From the specimen F3348, only the forelimb has been described (Wade, 1984).

From Colombia, the upper Barremian specimen CIP-GA-01042014, a nearly complete skeleton including the left forelimb, referred by Maxwell et al. (2019) to *P. sachicarum* ("*Kyhytysuka*" *sachicarum* in Cortés et al., 2021), includes a complete but poorly preserved skull. This skull is badly fractured, and many of the morphological features are hardly recognizable (Maxwell et al., 2019). Nevertheless, in addition to the similarities shared with the holotype, noted by Maxwell et al. (2019), some features (discussed below) allow us to confirm the species assignation of CIP-GA-01042014 to *P. sachicarum*.

In summary, the cranial morphology of the specimens preserving forelimb typical of *Platypterygius* associated to skull remains is still partially known. Nevertheless, the cranial features that can be compared, such as the proportions of the snout, orbital and postorbital regions, size, and position of the external nares, elongation of the maxilla, shape of the basioccipital and morphology of the teeth are concurrent in these specimens. The shared features are not exclusive to *Platypterygius*, but their combination distinguishes it from other Cretaceous ophthalmosaurids. Based on these features, some cranial remains not associated with forelimbs were identified as *Platypterygius*, as the holotype of *P. sachicarum* (Páramo, 1997), which was identified when appendicular remains from Colombia were not yet known. Now, the two Colombian specimens found in the same stratigraphic levels (CIP-GA-01042014 and FCG-CBP-87), preserving forelimb remains showing *Platypterygius* type morphology, support the presence of this genus in the Barremian beds of the Arcillolitas abigarradas Member of Colombia (Cortés & Páramo-Fonseca, 2018; Maxwell et al., 2019). Likewise, several Australian cranial remains have been identified as *Platypterygius australis* (Kear, 2005; Kear & Zammit, 2014; McGowan, 1972; Wade, 1984; 1990; Zammit, 2010; Zammit et al., 2010), by their affinity with those specimens preserving associated skull and forelimb remains. In the same way, German cranial material was identified as *Platypterygius hecynicus* (Fischer, 2012; Kolb & Sander, 2009) and some North American as *Platypterygius americanus* (Maxwell & Kear, 2010; McGowan, 1972). All this cranial material has enhanced the knowledge of the cranial morphology of *Platypterygius*. The following cranial features of *Platypterygius* differ from other Cretaceous ophthalmosaurids.

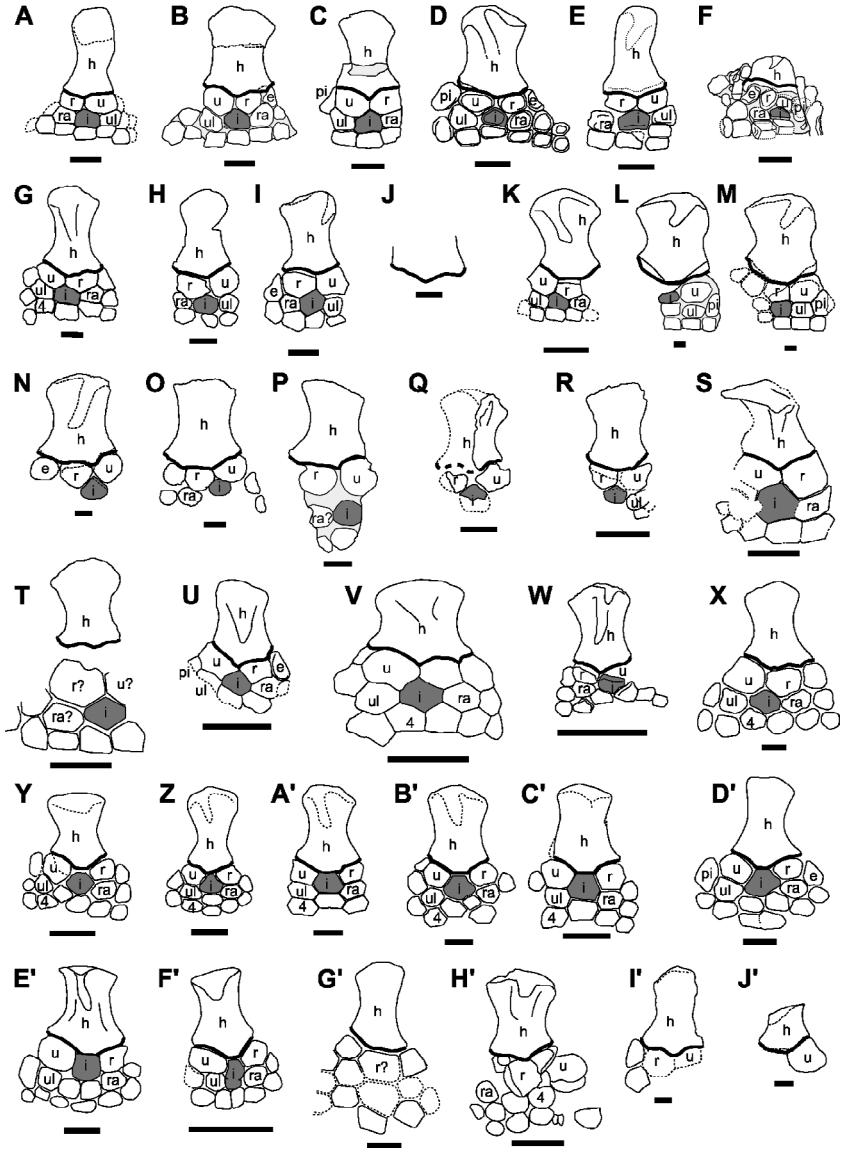

Figure 2. Comparison of the humerus and carpal structure of the ophthalmosaurids (and the Cretaceous thunnosaurian *Malawania anachronus*). In all the figures we eliminate the distal elements of the forelimb for facilitating the comparison. **A,** *Platypterygius platydactylus* left forelimb in dorsal view (from Broili, 1907); **B,** *Platypterygius australis* QM F2453, left forelimb in ventral view (from Zammit et al., 2010); **C,** *Platypterygius americanus* UW 2421 right forelimb in dorsal view (from McGowan, 1972); **D,** *Platypterygius hercynicus* SGS, right forelimb in dorsal view (from Kolb & Sander, 2009); **E,** *Platypterygius sachicarum* CIP-GA-01042014, left forelimb in dorsal view (from Maxwell et al., 2019); **F,** *Platypterygius sp.* FCG-CBP-87, left forelimb in dorsal view (from Cortés & Páramo-Fonseca, 2018); **G,** *Undorosaurus nessovi* UPM EP-II-24(785), right forelimb in dorsal view; **H,** *Undorosaurus gorodischensis* UPM EP-II-21(1075), left forelimb in dorsal view (from Zverkov & Efimov, 2019); **I,** *Undorosaurus gorodischensis* PMO 214.578, left forelimb in dorsal view (from Zverkov & Efimov, 2019); **J,** *Sisteronia seeleyi* CAMSM B58257_67, left humerus in dorsal view (from Fischer et al., 2014a); **K,** *Maiaspondylus cantabrigiensis* ZIN, ZIN PH 1/71, right forelimb in dorsal view (from Zverkov & Grigoriev, 2020); **L,** *Maiaspondylus lindoei* holotype UALVP 45635, left forelimb in dorsal view (from Maxwell & Caldwell, 2006a); **M,** *Maiaspondylus lindoei* holotype UALVP 45635, left forelimb in dorsal view (from Zverkov & Grigoriev, 2020); **N,** *Arthropterygius chrisorum* CMN 40608, left forelimb in dorsal view (from Maxwell, 2010); **O,** *Arthropterygius lundi* PMO 222.654, left forelimb in dorsal view (from Zverkov & Prilepskaya, 2019); **P,** *Arthropterygius thalassonotus* MOZ-PV 6145, right forelimb in ventral view (from Campos et al., 2019); **Q,** *Acuetzpalin carranzai* IGM 9519, left forelimb in ventral view (from Barrientos-Lara & Alvarado-Ortega, 2020); **R,** *Nannopterygius enthekiodon* NHMUK PV 46497, left forelimb in dorsal view (from Zverkov & Jacobs, 2020); **S,** *Malawania anachronus* NHMUK PV R6682, right forelimb in dorsal view (from Fischer et al., 2013); **T,** *Myobradypterygius hauthali* MLP 79-I-30-1, humerus in dorsal view and MLP 79-I-30-2, fragment of a forelimb (from Fernández & Aguirre-Urreta, 2005); **U,** *Sumpalla argentina* MOZ-PV 5788, right forelimb in dorsal view (from Campos et al., 2021); **V,** *Catutosaurus gaspariniae* MOZ-PV-1854, right forelimb in ventral view (from Fernández et al., 2021); **W,** *Sveltonectes insolitus* IRSNB R269, left forelimb in dorsal view (from Fischer et al., 2011); **X,** *Ophthalmosaurus icenicus* NHMUK PV R3702, right forelimb in dorsal view (from Moon & Kirton, 2016); **Y,** *Brachypterygius extremus* BRSMG Ce 16696*,* **Z,** *Otschevia pseudoscythicus*, **A',** *O. zhuravlevi*, **B',** *O. alekseevi*, **C',** *Otschevia cf. zhuravlevi UPM 2887/1-37*, forelimbs in dorsal view (from Zverkov et al., 2022 under the name *Grendelius*); **D',** *Brachypterygius extremus*, right forelimb in dorsal view (from McGowan, 1997); **E',** *Parrassaurus yacahuilztli* CPC 307, reconstructed right forelimb in dorsal view (from Barrientos-Lara & Alvarado-Ortega, 2021b); **F',** *Aegirosaurus leptospondylus* SM, right forelimb in dorsal view (from Bardet & Fernández, 2000); **G',** *Caypullisaurus bonapartei* MACN-N-32, reconstructed forelimb (from Fernández, 1997); **H',** *Thalassodraco etchesi* K1185, right forelimb in dorsal view (from Jacobs & Martill, 2020); **I',** *Gengasaurus nicosiai* MSVG 39617, left? forelimb in dorsal view (from Paparella et al., 2016); **J',** *Acamptonectes densus* holotype GLAHM 132588, right forelimb in ventral view (from Fischer et al., 2012). Abbreviations: **e**, anterior accessory epipodial element; **h**, humerus; **i**, intermedium; **pi**, pisiform; **r**, radius; **ra**, radiale; **u**, ulna; **ul**, ulnare. To visually compare the proportions of the fin elements, we scaled all the humerus to the same proximodistal length of the humerus. Scale bars = 50 mm.

The skull of *Platypterygius* is large, surpassing 70 cm in length, differing from *Sveltonectes* and *Muiscasaurus*, in which the skull is no longer than 65 cm (Fischer et al., 2011; Maxwell et al., 2016; Páramo-Fonseca et al., 2021). The general shape of the skull of *Platypterygius* has an almost straight dorsal and ventral margins in lateral view (Fig. 3A) (Kear, 2005, figs. 1–2; Páramo, 1997, fig. 2; Romer, 1968, fig. 2; Wade, 1984, fig. 1; 1990, fig. 3), differing from *Muiscasaurus*, *Athabascasaurus*, *Sveltonectes*, and *Leninia*, in which the skull is vaulted or curved above the orbit (Druckenmiller & Maxwell, 2010, fig. 11; Fischer et al., 2013, fig. 3; Páramo-Fonseca et al., 2021, fig. 3). The snout in *Platypterygius* is elongated, and the orbit is proportionally small with respect to the mandibular length (0.15-0.16) (Fig. 3A) (Kear, 2005, figs. 1–2; Páramo, 1997, fig. 2; Romer, 1968, fig. 2; Wade, 1984, fig. 1; 1990, fig. 3). This proportion differs from the larger orbit found in *Muiscasaurus* (0.22) and *Sveltonectes* (0.18) (Fischer et al., 2011, fig. 1; Páramo-Fonseca et al., 2021, figs. 2–3) and is unknown in other Cretaceous ophthalmosaurids. The postorbital region of *Platypterygius* is proportionally extensive regarding the orbital length (0.45-0.60) (Fig. 3A) (Kear, 2005, figs. 1–2; Páramo, 1997, fig. 2; Romer, 1968, fig. 2; Wade, 1984, fig. 1; 1990, fig. 3). The postorbital region is also large in *Athabascasaurus* (0.45) (Druckenmiller & Maxwell, 2010, fig. 11), but is shorter in *Muiscasaurus* (0.27), *Sveltonectes* (approximately 0.30) and *Leninia* (0.27) (Fischer et al., 2011, fig. 1; 2013, fig. 3; Páramo-Fonseca et al., 2021, fig. 3), and is unknown in other Cretaceous ophthalmosaurids.

In *Platypterygius*, the external naris is widely separated from the orbit (Fig. 3A) (Kear, 2005, figs. 1–2; Páramo, 1997, fig. 2; Romer, 1968, fig. 2; Wade, 1984, fig. 1; 1990, fig. 3), as in *Caypullisaurus*, *Athabascasaurus*, and "*Simbirskiasaurus*" (Druckenmiller & Maxwell, 2010, figs. 5, 6 and 11; Fernández, 1997; 2007; Fischer et al., 2014c, fig. 1), and differs from *Muiscasaurus* and *Leninia*, in which the naris is closer to the orbit (Fischer et al., 2013, fig. 3; Páramo-Fonseca et al., 2021, fig. 3). In *Platypterygius* the naris is divided into an anterior and a posterior opening by a naso-maxillar pillar (Fig. 3A) (Cortés et al., 2021 as "*Kyhytysuka*"; Kear, 2005; Páramo, 1997; Romer, 1968). Such a naso-maxillar pillar is only shared with "*Simbirskiasaurus*" (Fischer et al., 2014c) and is absent in all other Cretaceous ophthalmosaurids for which the naris is known, nonetheless, this feature is also present in Upper Jurassic taxa, such as *Arthropterygius thalassonotus* Campos *et al.*, 2020.

The supratemporal process of the parietal is broad and short in *Platypterygius* (Fig. 3B) (Kear, 2005, fig. 2; Wade, 1984, fig. 1) differing from *Sveltonectes*, *Athabascasaurus, Leninia* and *Plutoniosaurus* in which this process is relatively slender or elongated (Druckenmiller & Maxwell, 2010; Fischer et al., 2011; 2013; Zverkov & Efimov, 2019 dataset). The anterior exposure of the maxilla vastly exceeds the level of the external naris in *Platypterygius* (more than 1.5 times the complete external naris length) (see Fig. 3A) (Fischer, 2012; Kear, 2005; Páramo, 1997; Romer, 1968; Wade, 1984; 1990). This trait differs from *Muiscasaurus*, *Sveltonectes* and *Maiaspondylus*, in which the anterior extension of the maxilla is shorter (less than 1.5 times the external naris length) (Fischer et al., 2011; Maxwell & Caldwell, 2006a, Pl. 1, fig. 1; Páramo-Fonseca et al., 2021). The quadratojugal of *Platypterygius* has an extensive to moderate lateral exposure (Fig. 3A) (Fischer, 2012; Kear, 2005; Páramo, 1997; Romer, 1968), differing from *Muiscasaurus* in which the quadratojugal is greatly reduced (Páramo-Fonseca et al., 2021). No squamosal is found in *Platypterygius*, whereas it is present in *Caypullisaurus*, *Leninia*, *Athabascasaurus*, and *Muiscasaurus* (Druckenmiller & Maxwell, 2010; Fernández, 1997; 2007; Fischer et al., 2013; Páramo-Fonseca et al., 2021). In the remaining Cretaceous ophthalmosaurids this trait is unknown.

The extracondylar area of the basioccipital, generally taken to be extremely reduced in all *Platypterygius*, actually varies from reduced, as in *P. platydactylus* (Broili, 1907, Taf. XIII, fig. 5), to practically absent, as in *P. australis* (Kear, 2005, fig. 10A) (Fig. 3C). A reduced condition is found in most of the Cretaceous ophthalmosaurids, but in *Acamptonectes* Fischer et al., 2012 and *Leninia*, the extracondylar area is larger (Fischer et al., 2012; 2013). The angular and surangular in *Platypterygius* have a subequal lateral exposure (Fig. 3A), differing from *Athabascasaurus* in which the angular is more exposed than the surangular (Druckenmiller & Maxwell, 2010).

The teeth of *Platypterygius*, with conical crown and quadrangular root (Cortés et al., 2021 as "*Kyhytysuka*"; Kear, 2005; Kuhn, 1946; Páramo, 1997; Romer, 1968) do not differ from most Cretaceous ophthalmosaurids. However, in *Platypterygius* the crown is stout and has ridges along the entire enamel (Fig. 3D) (Kear, 2005; Kuhn, 1946; Páramo, 1997; Romer, 1968), which differs from the gracile or slender crown of *Sisteronia* Fischer et al., 2014a (Fischer et al., 2014a) and *Athabascasaurus* (Druckenmiller & Maxwell, 2010) and the smooth or lightly ridging crown of *Maiaspondylus* (Maxwell & Caldwell, 2006a) and *Athabascasaurus* (Druckenmiller & Maxwell, 2010).

Thus, the species showing the typical forelimb of *Platypterygius* also share a particular skull morphology, which supports their inclusion in a separate genus. This morphology shows a particular combination of features which is not present in any other Cretaceous ophthalmosaurid except "*Simbirskiasaurus*" in which the features that can be compared concurs with the *Platypterygius* skull morphology.

"*Simbirskiasaurus*" is known from a single specimen that consists of a portion of a three-dimensionally preserved skull and some vertebrae (Fischer et al., 2014c; Ochev & Efimov, 1985). The features of this specimen concur with the discussed cranial morphology of *Platypterygius*: the length of the skull is estimated at more than 70 cm; the preserved portion of the skull does not show a vaulted dorsal margin above the orbit; the external naris is widely separated from the orbit and divided into an anterior and a posterior opening by a naso-maxillar pillar; the basioccipital has an extremely reduced extracondylar area; and the tooth crown is robust and textured with apicobasal ridges (Fischer et al., 2014c; Ochev & Efimov, 1985). Five of the six cranial features proposed by Fischer et al. (2014c) as diagnostic for "*Simbirskiasaurus*" are found in *Platypterygius*. These features are: The already discussed divided external naris that is typical in *Platypterygius*; an interdigitating prefrontal-lacrimal suture that is found in *P. australis* (Kear, 2005) and *P. sachicarum* (personal observation), and is unknown or poorly preserved in other *Platypterygius* species; an elongated anterior process of the maxilla which is present in *P. americanus* and *P. sachicarum* (Páramo, 1997; Romer, 1968) and unknown in other *Platypterygius* species; a supranarial process of the premaxilla that is found in *P. australis* and *P. americanus* (Kear, 2005; Romer, 1968) and is unknown or poorly preserved in other *Platypterygius* species; a dorsal extension in the posterior opening of the narial complex, which although no anteroposteriorly constricted, is found in *P. americanus* and *P. australis* and to a lesser degree in *P. sachicarum* (Kear, 2005, figs. 1-4; Páramo, 1997, figs. 2-3; Romer, 1968, fig. 3). The sixth diagnostic character, an elongated subnarial process of the premaxilla, is found in *P. australis* and *P*, *americanus*, although not reaching the posterior margin as in "*Simbirskiasaurus*" (Kear, 2005; Romer, 1968). We consider these minor cranial differences not sufficient to justify a generic distinction and therefore, we follow Maisch & Matzke (2000) and McGowan and Motani (2003) in considering "*Simbirskiasaurus*" a junior synonym of *Platypterygius*.

Cortés et al. (2021) erected the new genus name "*Kyhytysuka*" to differentiate *P. sachicarum* from *P. platydactylus* (as the type species of *Platypterygius*) based on some cranial differences that the authors noted between the holotype of "*K.*" *sachicarum* and that of *P. platydactylus*. These differences refer to the ventral curvature of the mandible, the dorsal projection of the almost imperceptible coronoid process, the inclination of the retroarticular process of the mandible, the posterior extension of the angular and the proportions of the quadrate condyle. Considering that some of these features assumed for *P. platydactylus* may result from the orientation of the drawing in the figures of Broili (1907) or reflect preservation features of the specimen, we consider that the minor cranial differences noted by Cortés et al. (2021) are not sufficient evidence for a generic distinction. Moreover, Cortés et al. (2021) recognized as "*K.*" *sachicarum* the Colombian specimen CIP-GA-01042014, which preserves a forelimb typical of *Platypterygius* (see above), but surprisingly, they do not discuss the morphological affinities of this forelimb with that of the type species *P. platydactylus*. The forelimb morphology of this specimen shows us once again that there is no solid evidence for a generic distinction between "*Kyhytysuka*" and *Platypterygius* and therefore, we here reassign "*K.*" *sachicarum* to *Platypterygius sachicarum*.

In summary, *Platypterygius* is here recognized as a genus, distinguished from other ophthalmosaurids not only by its typical forelimb morphology but also by its particular combination of skull features. Minor differences in traits such as the enlargement of the maxilla, angular, surangular or the premaxillary processes, size, and shape of the external narial apertures, the extension of the extracondylar area of the quadrate, the robustness of the stapes, the number of maxillary teeth, among others, support the distinction of different species within the genus (Broili, 1907; Fischer et al., 2014c; Kear, 2005; Kolb & Sander, 2009; Kuhn, 1946; Romer, 1968; Páramo, 1997).

The presence of diverse species of *Platypterygius* in distinct geographic regions (South America, North America, Europe, and Australia), coming from lower Barremian to lower Cenomanian beds, shows that *Platypterygius* was a successful genus, which diversified as it conquered the waters of the Early to early Late Cretaceous oceans and seas. As previously suggested by Maxwell & Caldwell (2006b), the occurrence of *Platypterygius* as a cosmopolitan genus could be expected due to its pelagic free-swimmer condition.

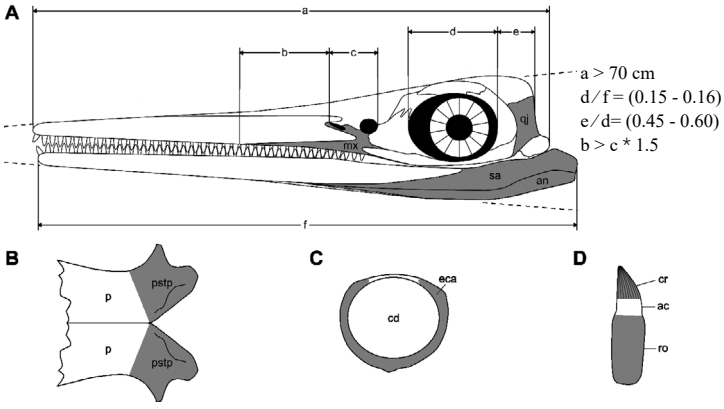

Figure 3. Schematic diagrams of a *Platypterygius* skull showing the cranial features, linear measurements, and skull ratios that differentiate this genus from other Cretaceous ophthalmosaurids. **A,** skull in left lateral view. **B,** parietals in dorsal view showing a broad and short supratemporal process. **C,** basioccipital in posterior view showing a reduced extracondylar area. **D,** tooth showing a stout crown with ridges along the entire enamel. Measurements: **a,** skull length; **b,** distance from the anterior tip of the maxilla to the anterior margin of the anterior narial opening; **c,** external naris length; **d,** orbit length; **e,** postorbital region length; **f,** mandibular length. Abbreviations: **ac,** acellular cementum; **an,** angular; **cd,** condyle; **cr,** crown; **eca,** extracondylar area; **mx,** maxilla; **p,** parietal; **pstp,** parietal supratemporal process; **qj,** quadratojugal; **ro,** root; **sa**, surangular.

Systematic paleontology

ICHTHYOSAURIA de Blainville, 1835
OPHTHALMOSAURIDAE Baur, 1887
Platypterygius Huene, 1922

Myopterygius Huene, 1922: 98
Longirostria Arkhangelsky, 1998: 612
Tenuirostria Arkhangelsky, 1998: 612
Simbirskiasaurus Ochev & Efimov, 1985: 88; Fischer et al., 2014c: 825.
Kyhytysuka Cortés et al., 2021: 2.

Type species: *Platypterygius platydactylus* (Broili, 1907)

Included species *P. platydactylus, P. americanus*, *P. australis*, *P. hercynicus*, *P. sachicarum*, *P. birjukovi* and a new species *P. elsuntuoso* here described.

Revised diagnosis: *Platypterygius* species share the following three synapomorphic features (autapomorphies for the genus): 1- Distal end of the humerus with articular facets for the ulna and the radius distally oriented, almost in the same plane and with reduced facet for extrazeugopodial elements, sometimes hardly noticeable; 2- intermedium roughly pentagonal with proximal pointed edge, nearly parallel anterior and posterior sides and longer and straight distal side; and 3- intermedium fitting between the radius and ulna and contacting almost exclusively radiale, ulnare and distal carpal 3.

Platypterygius is also distinguished by the following combination of characters: Skull with almost straight dorsal and ventral margins in lateral view, with orbit proportionally small in comparison to the mandibular length (0.15-0.16) and postorbital region proportionally extensive regarding to the orbital length (0.45-0.60) (also found in *Brachypterygius*, *Otschevia* and *Caypullisaurus*); external naris widely separated from the orbit and divided into an anterior and a posterior opening by a naso-maxillar pillar (also in *Arthropterygius thalassonotus* and roughly similar in *Maiaspondylus lindoei* Maxwell & Caldwell, 2006a and *Parrassaurus*); supratemporal process of the parietal robust and short (also in *Caypullisaurus* and *Acuetzpalin*); quadratojugal with extensive or moderate lateral exposure (also in *Caypullisaurus* and *Athabascasaurus*); tooth crown stout and having ridges along the entire enamel (also in *Brachypterygius*, *Parrassaurus*, and *Arthropterygius hoybergeti* (Druckenmiller et al., 2012); atlas-axis with ventral keel (also in *Acamptonectes*); coracoid with a poorly pronounced anteromedial process (differing from *Caypullisaurus*, *Sveltonectes*, and *Acamptonectes*); humerus with massive deltopectoral crest, matching in height the trochanter dorsalis (also in *Acuetzpalin* and *Sveltonectes*); intermedium not contacting the humerus (differing from *Otschevia* spp., *Brachypterygius*, *Parrassaurus*, and *Aegirosaurus*); radiale and ulnare articulating distally almost exclusively with a single distal carpal, and contact between proximal and distal carpals 2, 3 and 4 in a near straight line (also in *Undorosaurus* spp. and *Maiaspondylus* spp.); proximal forelimb phalanges rectangular and closely fitting (also in *Sveltonectes*, *Caypullisaurus Maiaspondylus* spp. and *Aegirosaurus*); digital count not less than 7 producing a broad fin by hyperdactyly (also in *Caypullisaurus* and *Maiaspondylus lindoei*).

Platypterygius elsuntuoso sp. nov.
urn:lsid:zoobank.org:act:2A6F34A9-5D10-447D-9CAD-B5848ECC0CF9

Holotype and only known specimen: FCG-CBP-28. A skull lacking the anterior portion of the snout; some disarticulated axial elements, incomplete left coracoid, and a few phalanges.

Type locality and horizon: Loma La Cabrera, northwest of Villa de Leiva, Boyacá. Paja Formation, Arcillolitas abigarradas Member, segment A or B of Etayo-Serna (1968a), lower Barremian (Benavides-Cabra et al., 2023) (Fig. 1).

Derivation of name: from "el suntuoso", Spanish for "the sumptuous", nickname used by C. B. Padilla, deceased founder of the FCG and CIP, when referring to the specimen.

Diagnosis: *P. elsuntuoso* is distinguished from other species of *Platypterygius* by the following unique features: 1- The anterior ventral border of the extracondylar area of the basioccipital bears a small ventral peg anteroventrally directed (Shared with *Plutoniosaurus*, Zverkov pers. comm.), which fits into a posteroventral depression found in the basisphenoid; 2- Quadrate with supratemporal groove dorsal to the stapedial foramen (Shared with *Plutoniosaurus* Zverkov pers. comm.; and *Undorosaurus* see Zverkov & Efimov, 2019) ; and 3- Root of teeth with a shallow neck at the base of the acellular cementum ring.

P. elsuntuoso is also characterized by the following combination of features: Supranarial process of the premaxilla relatively short (larger in *P. americanus*); subnarial process of the premaxilla not reaching the posterior margin of the posterior narial opening (reaching posterior narial margin in *P. birjukovi*); maxilla with no extensive anterior projection (extremely extensive in *P. americanus* and *P. sachicarum*); external exposed maxilla bearing 18 teeth (more than 20 teeth in *P. americanus*, *P. australis*, and *P. sachicarum*); pineal foramen surrounded exclusively by frontal processes (surrounded by frontals and parietals in *P. australis*); lacrimal reaching the external narial margin (separated to the narial margin by the maxilla in *P. australis*); supratemporal contacting the postorbital (not contacting in *P. americanus*) and with a long anterolateral process (shorter in *P. hercynicus* and *P. australis*); extensive lateral exposure of the quadratojugal (lesser exposed in *P. hercynicus*); extracondylar area of the basioccipital reduced but present laterally and ventrally (extremely reduced in *P. australis* and *P. birjukovi*); long basipterygoid processes of the basisphenoid (shorter in *P. platydactylus* and *P. australis*); opisthotic facet of the basioccipital laterodorsally directed (more dorsally and anteriorly directed in *P. australis* and *P. hercynicus*); long stapes (shorter *in P. platydactylus* and *P. australis*); teeth with vertical grooves basal to the crown and apical to the root osteocementum (also in *P. sachicarum;* without vertical grooves in *P. hercynicus*, *P. birjukovi*, and *P. australis*); rugose apical texture in teeth (shared with *P. sachicarum*); atlas-axis suture visible externally (no visible externally in *P. platydactylus*, *P. americanus*, and *P. australis*).

4. Description

Preservation features

The specimen was found enclosed in seven blocks of a large concretion containing a skull and some postcranial remains three-dimensionally preserved (Fig. 4). The blocks are separated by natural transverse fractures that offer cross-sectional exposure of the bones. The skull lacks a large portion of the anterior

end and is better preserved on its right lateral side (Fig. 4A). Nevertheless, on this side, the narial region is broken. The left side of the skull is displaced forward and consequently many bones are distorted and fractured (Fig. 4B). The greatest effects of erosion also occurred on this side. The description is therefore based on the right side of the skull, which does not show signs of diagenetic deformation.

The bones of the braincase are preserved out but near their anatomical position, whereas the palatal bones are mostly displaced from their original position (Fig. 4B). Four disarticulated cervical centra, two neural arches with preserved neural spines and some rib fragments are preserved in the posterodorsal region and posterior left side of the skull (Fig. 4B, C). In the posteroventral region of the skull some elements of the appendicular skeleton (the left coracoid and six phalanges) can be identified (Fig. 4B). The basioccipital and the coracoid were extracted during the preparation to better understand their morphology.

Ontogeny

The relation between the orbital area and the area occupied by the sclerotic ring was proposed to be indicative of the ontogenetic stage in ophthalmosaurid ichthyosaurs (Fernández et al., 2005). In FCG-CBP-28 the sclerotic ring area represents 83% of the orbital area (Fig. 4A), suggesting a juvenile to subadult stage of the individual (following Fernández et al., 2005). The aperture area in FCG-CBP-28 is approximately 14% of the orbital area (Fig. 4A), a value lower than the 20% proposed for juvenile specimens and closer but higher to the values found in adult specimens (Fernández et al., 2005). This condition supports a subadult stage for the specimen FCG-CBP-28. FCG-CBP-28 shows a raised ridge in the ventral margin of the stapedial facet of the quadrate (Fig. 5E-G). Following Moon & Kirton (2016), a stapedial facet ridge is prominent and ventrally tuberous in well ossified individuals of *Ophthalmosaurus*. That implies the specimen FCG-CBP-28 was an ossified individual, not a juvenile. The atlas-axis complex of FCG-CBP-28 retains external vestigial suture between the two elements, but is internally well fused (Fig. 9A, B), supporting the idea of an individual with a not completely ossified skeleton.

Skull

Given that the anterior end of the snout is lost, we cannot give a complete measurement of the skull. As preserved, the length of the skull (from the posterior end of the quadrate) is 86.5 cm (Fig. 4). Based on a graphic anterior projection of the dorsal margin of the skull, the ventral margin of the mandibles and the upper and lower alveolar margins, we estimate the skull length to be approximately 123 cm. Based on this estimate, the snout length was approximately 103 cm, that is 4.7 times the orbital diameter, and the estimated orbital ratio is 0.15 (ratio proposed by McGowan & Motani, 2003). The orbit is undeformed and has a slightly elliptical outline. Although the narial region is broken, the margin of the anterior narial opening is well-defined on the right side of the skull (Fig. 4A). The distance between the posterior end of the quadrate condyle to the anteriormost border of the external naris is 45 cm. The postorbital region (taken from the posterior orbital margin to the level of the posterior end of the quadrate condyle) is large, it represents 61.5 % of the orbital horizontal diameter.

The shape and size of the preserved margin of the anterior narial opening on the maxilla and the disposition of the surrounding bones (Fig. 4A) allows inferring that the anterior narial opening was oval and was posteriorly limited by a pillar formed by the nasal and the maxilla. Nothing can be described about the shape of the posterior narial opening because of the bad preservation of this region on both sides of the skull. Nevertheless, on the left side of the skull a descending process of the nasal forms at least a portion of the posterior margin of the posterior narial opening (Fig. 4B; 5B).

Cranium

Premaxilla: The premaxillae lack the anterior portion and are broken at their posterior end, so the morphology of the narial processes remains doubtful. The preserved portions of the processes suggest a small supranarial process that ends at the level of the posterior margin of the anterior narial opening and a dorsoventral high subnarial process that ends more posteriorly than the supranarial process. On the right side of the skull, between the broken premaxillary processes, the maxilla is exposed in lateral view forming the anterior margin of the anterior narial opening (Fig. 4A). Nonetheless, it is likely that the premaxilla formed the ventral, anterior, and part of the dorsal margins of the anterior narial opening, covering the maxilla externally. On the left side of the skull, although the bones in this region are somewhat fractured and displaced, the subnarial process of the premaxilla can be seen reaching the lacrimal (Fig. 4B; 5B). The lateral premaxillary canal is narrow and deep in the anterior region, it broadens and becomes shallower at the level of the sixth tooth position anterior to the lateral emergence of the maxilla and disappears approximately at the level of the anterior end of the maxilla (Fig. 4A); it does not meet the external naris.

Nasal: The nasal is very extended anteriorly making at least 44% of the estimated snout length. The nasal limits posteriorly with the frontal and the postfrontal and posterolaterally with the postfrontal and the prefrontal. The medial relationships of both nasals cannot be discerned due to the forward displacement of the left one. However, on the dorsal surface of the left nasal there is a wide medial concavity at the level of the external naris and a narrower one behind it. The nasal does not have a lateral wing over the external naris (Fig. 4A, B; 5B). In the lateral narial region, the right nasal is broken. Nonetheless, on the left side of the skull the nasal clearly shows a descending process posterior to the posterior narial opening and some broken fragments of bone are found where the nasomaxillary pillar should have been found (Fig. 4B; 5B).

Frontal: Both frontals are preserved. The right one, although preserved in its anatomical position, is slightly dorsomedially inclined, and the left one is displaced forward in relation to the right one (Fig. 4C). The frontal contacts the nasal anteriorly in an interdigitated suture, and laterally, it contacts the prefrontal. The frontal participates in the anteromedial margin of the temporal fenestra, contacting laterally the postfrontal (Fig. 4C). A thickened posterior process of the frontal overlaps the parietal forming the anterior, lateral, and the posterior margin of the parietal foramen.

Parietal: The right parietal is preserved in its anatomical position, although rotated, with its medial side turned dorsally. From the left side of the skull, only some undetermined parietal fragments are recognized (Fig. 4B, C). The parietal is wide; it is anteriorly covered by the temporal process of the frontal, and posteriorly it overlaps the anterior projection of the supratemporal (Fig. 4C). The parietal forms the posterior medial margin of the temporal fenestra. Due to the crushing of the left side of the skull, only the right side of the parietal foramen can be seen. Since this foramen is exposed in medial view, it is observed that the parietal forms the internal wall of the foramen, but the frontal, overlapping the parietal, forms the external margins of the parietal foramen. This foramen is oval-shaped (4.0 cm long) and is located behind the level of the anterior margin of the temporal fenestra (Fig. 4C).

Maxilla: The anterior process of the maxilla is largely exposed in lateral view; it extends beyond the level of the naris, between 1.5 and 2.4 times according to the range of the estimated narial length (including the anterior opening) and slightly exceeds the level of the lateral exposure of the nasal. Its anterior end is located at 1.67 times the orbital length from the anterior orbital margin. The lateral exposure of the posterior end of the maxilla does not reach the level of the anterior end of the orbit because it is covered by the jugal (Fig. 4A). The maxilla extends dorsally surrounding the anterior narial opening medial to the premaxilla. The maxilla broadly contacts the ventral border of the lacrimal. The posterior dorsal end of the maxilla remains unknown. The ventral border of the maxilla is concave and laterally participates in the construction of the dental canal through 18 functional positions.

Lacrimal: The lacrimal is anteroposteriorly long and seems to have reached the posterior end of the subnarial process of the premaxilla. Dorsally, it contacts the prefrontal in a suture that is deeply interdigitated in the orbit rim. Ventrally, it contacts the jugal posteriorly and the maxilla anteriorly. Although the posterior narial opening is not preserved, the dorsal and ventral limits of the lateral exposure of the lacrimal (Fig. 4A, B; 5B) indicate that it reached the external naris.

Prefrontal: The anterior end of the prefrontal is broken. Its anteriormost preserved portion is dorsoventrally high close to the position where the posterior narial opening should start. However, in the damaged region the nasal descends as forming the posterodorsal edge of the posterior opening, so it cannot be assured that the prefrontal reached the posterior narial opening in lateral view. On the left side of the skull, the prefrontal is slightly displaced from its original position, but it preserves the anterior end (Fig. 4B; 5B). This end is located near a descending process of the nasal, which supports the interpretation that the prefrontal does not reach the posterior margin of the naris, at least in lateral view.

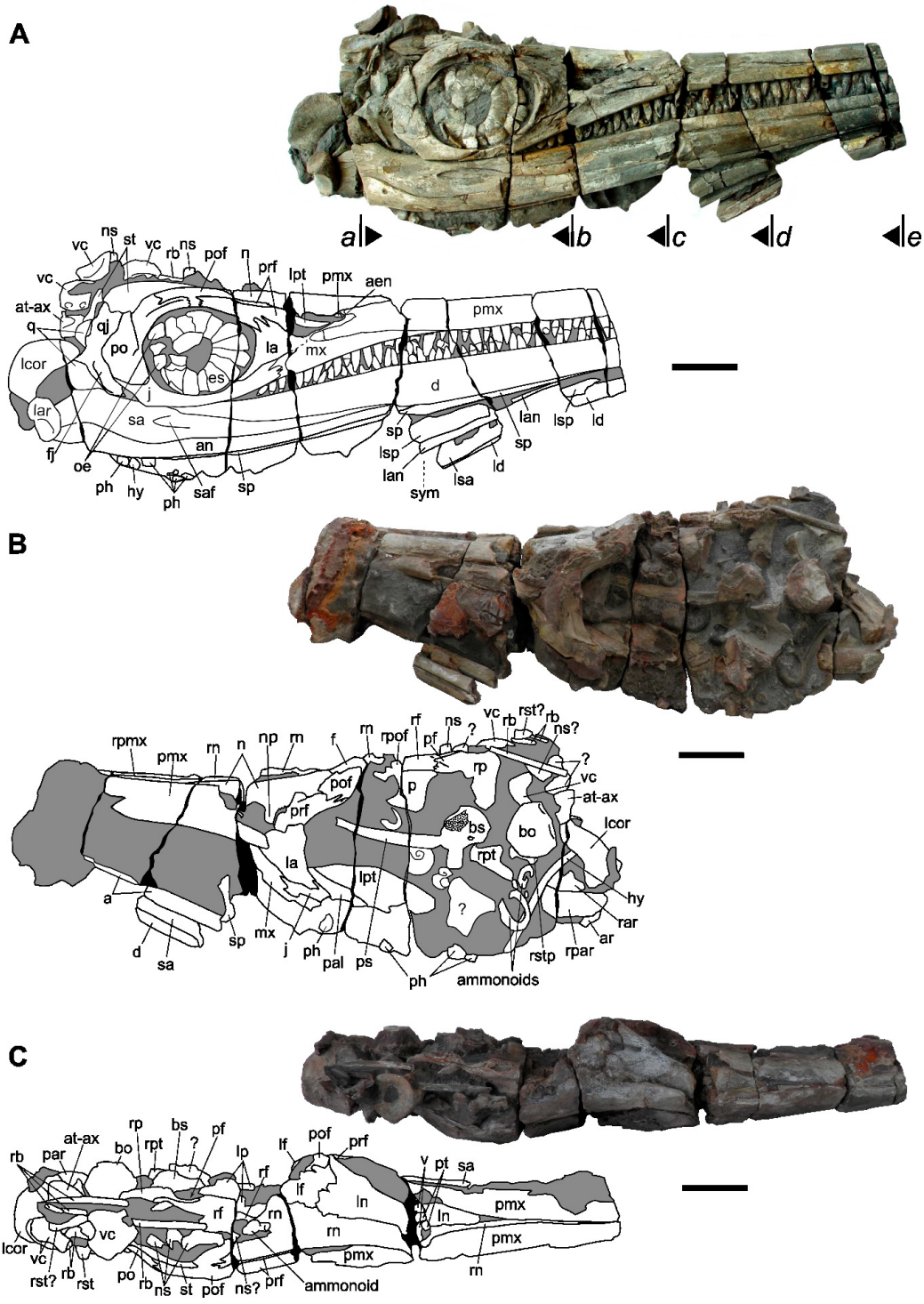

Figure 4. *Platypterygius elsuntuoso* sp. nov., holotype FCG-CBP-28. Photographs and interpretative drawings of the specimen in **A**, right lateral view, **B**, left lateral view before extracting the basioccipital and the left coracoid, and **C**, dorsal view. Grey: sediment; black: breakage space; dots: missing surface. Abbreviations: **aen**, anterior external narial aperture; **an**, angular; **ar**, articular; **at**, atlas; **ax**, axis; **bo**, basioccipital; **bs**, basisphenoid; **d**, dentary; **es**, sclerotic plates; **f**, frontal; **fj**, facet for the jugal; **hy**, hyoid; **j**, jugal; **la**, lacrimal; **lan**, left angular; **lar**, left articular; **lcor**, left coracoid; **ld**, left dentary; **ln**, left nasal; **lpt**, left pterygoid; **lsa**, left surangular; **lsp**, left splenial; **mx**, maxilla; **n**, nasal; **np**, nasal process; **ns**, neural spine; **oe**, occipital element; **p**, parietal; **pal**, palatine; **par**, prearticular; **pf**, parietal foramen; **ph**, phalange; **pmx**, premaxilla; **po**, postorbital; **pof**, postfrontal; **prf**, prefrontal; **ps**, parasphenoid; **pt**, pterygoid; **q**, quadrate; **qj**, quadratojugal; **rb**, rib; **rar**, right articular; **rn**, right nasal; **rpar**, right prearticular; **rpt**, right pterygoid; **rst**, right supratemporal; **rstp**, right stapes; **sa**, surangular; **saf**, surangular fossa; **sp**, splenial; **st**, supratemporal; **sym**, posterior end of the symphysis; **v**, vomer; **vc**, vertebral centrum. Scale bars = 100 mm.

The prefrontal forms the anterior half of the dorsal orbital margin (Fig. 4). Posteriorly, it articulates with the postfrontal in the orbital margin and with the nasal dorsomedially. Anteroventrally, the prefrontal contacts the lacrimal forming an interdigitated suture (Fig. 4A).

Postfrontal: The postfrontal has a large dorsomedial process that participates in the anterior margin of the temporal fenestra (Fig. 4C). It is substantially excluded from the lateral border of the temporal fenestra by an anterior elongation of the supratemporal. The postfrontal underlaps the posterior end of the nasal and overlaps the dorsal portion of the prefrontal (Fig. 4). It forms a short portion of the orbital roof between the prefrontal and postorbital. Posterolaterally, the postfrontal broadly contacts the postorbital (Fig. 4A; 5A).

Jugal: The jugal forms one quarter of the posterior margin of the orbit (Fig. 4A). Anteriorly the jugal ends slightly anterior to the anterior orbital margin and posterior to the anterior margin of the lacrimal. The anterior end of the jugal is broad and overlaps the maxilla covering its entire height until the level of the third posterior maxillary tooth. The postorbital portion of the jugal is anteroposteriorly wide and is dorsally overlapped by the postorbital. A large facet for articulation in the quadratojugal indicates that the jugal articulates widely with the quadratojugal (Fig. 4A; 5A). The joining of the horizontal and vertical rami of the jugal forms an arched orbital margin and an angled ventral margin (Fig. 4A).

Postorbital: The postorbital is anteroposteriorly enlarged (Fig. 4A; 5A). It broadly contacts the supratemporal and forms almost a third of the dorsal orbital margin. Here, it develops a supraorbital crest (Fig. 5A). The postorbital is anterodorsally overlapped by the postfrontal, ventrally it overlaps the jugal and posteroventrally the quadratojugal.

Squamosal: There is no evidence of the presence of a squamosal bone.

Supratemporal: The supratemporal, although broken, is in anatomical position. It forms the posterior and almost the entire lateral margin of the temporal fenestra (Fig. 4C). Laterally it meets the postfrontal anteriorly and the postorbital posteriorly (Fig. 4A; 5A). It has a posterior descending ramus that contacts both the quadrate and the dorsal ramus of the quadratojugal. The lateral surface of the supratemporal exhibits a fine sub horizontal striate texture that contrasts with the vertical one of the ascending ramus of the quadratojugal and the oblique of the postorbital (Fig. 5A).

Quadratojugal: The quadratojugal, although in articulation with the quadrate, is slightly moved back; therefore, it exposes a strongly demarcated articular facet for the jugal and postorbital (Fig. 4A; 5A). The quadratojugal is a wide laminar bone, greatly exposed in lateral view, and it widely covers the quadrate externally. Ventrally, it broadly contacts with the dorsal surface of the quadrate condyle, and dorsally, it has an ascending ramus that is anteriorly overlapped by the postorbital. This ramus is fractured but can be recognized by its continuous texture (Fig. 4A). It dorsally touches the occipital lamella of the quadrate.

Quadrate: The quadrate is preserved in articulation with the mandible but slightly rotated dorsally from its anatomical position. The anteromedial region of the quadrate is embedded in sediment, and the posterodorsal region is obscured by the presence of the displaced atlas-axis complex; therefore, the pterygoid lamella is only partially exposed. Laterally, the quadrate is broadly covered by the quadratojugal, which contacts the quadrate on the dorsal surface of the articular condyle and on the occipital lamella (Fig. 4A; 5A). The quadrate is ear-shaped, with a large, massive articular condyle, in which two articular facets can be distinguished: a lateroventral facet articulating with the surangular and a posterior facet for the articulation with the articular (Fig. 4A; 5C, D). The occipital lamella curves posterolaterally giving the quadrate a concave distal edge. The stapedial facet is well exposed; it is a large deep concavity sub-circular in outline located in the lower half of the quadrate (Fig. 5E-G). The stapedial facet is surrounded by a raised ridge, which is more prominent ventrally. A raised ridge in the ventral margin of the stapedial facet was described for *Sveltonectes* by Fischer et al. (2011) and for *Maiaspondylus* spp. by Zverkov & Grigoriev (2020). Moon & Kirton (2016), noted that such a ridge is prominent and ventrally tuberous in well ossified individuals of *Ophthalmosaurus*. Inside the stapedial facet, a semi-ossified structure resembling a preserved membrane covers almost the complete area of the stapedial facet (Fig. 5F). Such a structure could represent an extrastapedial cartilage, as Kear (2005) interpreted for a similar structure in *Platypterygius australis* and can be compared to the extracolumella of some squamate reptiles (McDowell, 1967; Palci et al., 2020). Dorsal to the stapedial facet, a clearly demarcated groove is visible, probably representing a portion of a supratemporal groove (Fig. 5E, G).

Sclerotic ring

The sclerotic ring occupies almost the entire orbital cavity (Fig. 4A). It is formed by 15-16 sclerotic plates weakly imbricated. The peripheral portion of the sclerotic plates is thickened. The union between plates is interdigitated, zigzagging in cross-section. This suggests the sclerotic ring could expand, but there was no transverse mobility between the plates, giving a rather rigid protection to the eye.

Basicranium

From the basicranium, the basioccipital, basisphenoid-parasphenoid and the right opisthotic and stapes are visible. These elements were preserved disarticulated, but near their anatomical position. The basioccipital was extracted during preparation and thanks to this, the right opisthotic and stapes could be seen.

Basioccipital: The extracted basioccipital is plenty illustrated in a provided 3D model (see supplemental Data 1). It is not completely preserved; a portion of its anterodorsal region, including the anterior end of the foramen magnum floor, was lost due to erosion (Fig. 6B, C, E). In posterior and anterior views, the basioccipital is circular in outline with a flat dorsal surface. The extracondylar area is somewhat reduced but is well defined laterally and ventrally from the condyle. Anteroventrally, the extracondylar area is enlarged and bears a small ventral peg anteroventrally directed (Fig. 6B, D). This ventral peg fits into a posteroventral depression found in the basisphenoid. This feature has not been described before for other ophthalmosaurids. The preserved portion of the anterior surface of the basioccipital is convex, rugose and has a medial ventral shallow fossa anterior to the ventral peg. The floor of the foramen magnum is flat and elevated from the exoccipital facets (Fig. 6E). Posteriorly, the floor of the foramen magnum broadens and becomes slightly concave. Lateral to the foramen magnum floor, the facets for exoccipitals are well defined and have a nearly flat surface that slopes down anteromedially. The basioccipital condyle is nearly circular in outline and does not have a notochordal pit (Fig. 6A). The opisthotic and stapedial facets are well exposed in lateral view (Fig. 6C, F). The opisthotic facet is laterally oriented, and the stapedial facet is lateroventrally oriented. Both facets are subrectangular in outline and similar in size.

Basisphenoid-Parasphenoid: The basisphenoid is visible in its ventral and left lateral views and in a portion of its dorsal view (Fig. 4B; 6G-J). The parasphenoid is fractured just where it separates from the basisphenoid, and its anterior portion is slightly rotated (Fig. 6G, I, J). There is no trace of the suture between the basisphenoid and parasphenoid, but their junction is evident by the presence of a midline ventral ridge in the basisphenoid. In dorsal view, the basioccipital facet of the basisphenoid is similar in size to the dorsal plateau. The surface of the basioccipital facet is medially depressed and has a shallow furrow in its dorsal portion (the median furrow sensu McGowan & Motani, 2003) (Fig. 6H). The surface of the basioccipital facets curves ventrally forming a medial triangular furrow posteroventrally oriented that ends just behind the internal carotid foramen (Fig. 6I, J). This surface couples with the anteroventral peg of the basioccipital when they are articulated. The internal carotid foramen opens in the posterior third of the ventral surface of the basisphenoid (Fig. 6G, J). The basipterygoid processes are extremely large. They protrude from behind the anterior end of the body of the basisphenoid and largely extend anterolaterally, without surpassing the anterior end of the basisphenoid body. In lateral view (Fig. 6I), the facet for the stapes is exposed behind the basipterygoid process. It is posterolaterally oriented and occupies the dorsal two-thirds of the basisphenoid height. The parasphenoid cross-section changes from a triangular outline with the pointed end facing ventrally in its posterior region to an oval outline in its anterior portion.

Opisthotic: On the left side of the skull, the posterior view of the right opisthotic is exposed. The bone is found near its anatomical position; it is located behind the basisphenoid, dorsal to the stapes and lateral to the displaced basioccipital (Fig. 5G). The paraoccipital process of the opisthotic is short and robust. Proximally, the opisthotic expands and forms the articular facets for stapes, basioccipital and exoccipital (Fig. 5H). The facet for the basioccipital is the largest and that for the exoccipital is the smallest. These two facets are separated by a shallow channel-shaped depression comparable to that identified for *Ophthalmosaurus* as the jugular foramen by Appleby (1956, fig. 12) or the vagus foramen by Moon & Kirton (2016, figs. 12 and 16). The distal end of the paraoccipital process forms a broad condyle for the articulation with the supratemporal.

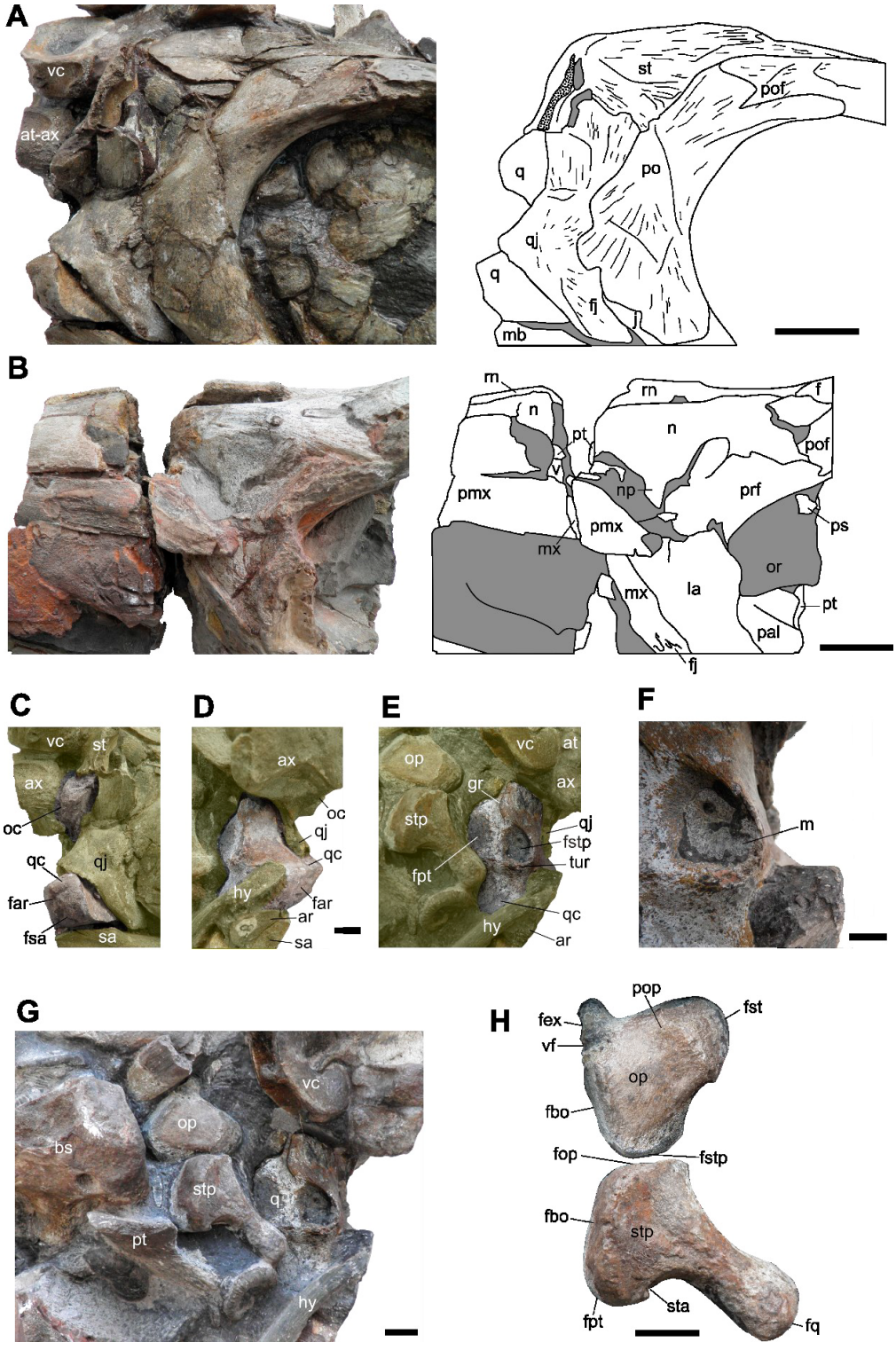

Figure 5. *Platypterygius elsuntuoso* sp. nov., holotype FCG-CBP-28. Skull details.
A, Photograph and interpretative drawing of the right temporal region in lateral view, showing the texture pattern in the different bones. **B**, Photograph and interpretative drawing of the left narial region in lateral view. **C-F**, quadrate in **C**, lateral, **D**, posterior and **E**, medial views; **F**, detail of the stapedial foramen on the quadrate showing a membranous structure into it. **G**, detail of the left posterior region of the specimen with disarticulated occipital elements. **H**, right stapes and opisthotic in posterior view, reconstructing their anatomical position. Grey: sediment; dots: missing surface; yellow shading: all surfaces that do not belong to the illustrated bone. Abbreviations: **ar**, articular; **at**, atlas; **ax**, axis; **f**, frontal; **far**, facet for the articular; **fbo**, facet for the basioccipital; **fex**, facet for the exoccipital; **fj**, facet for the jugal; **fop**, facet for the opisthotic; **fpt**, facet for the pterygoid; **fq**, facet for the quadrate; **fsa**, facet for the surangular; **fstp**, facet for the stapes; **gr**, groove; **hy**, hyiod; **j**, jugal; **la**, lacrimal; **m**, membranous structure (extrastapedial cartilage); **mb**, mandible; **mx**, maxilla; **n**, nasal; **np**, nasal process; **oc**, occipital crest of the quadrate; **op**, opisthotic; **or**, orbit; **pal**, palatine; **pmx**, premaxilla; **po**, postorbital; **pof**, postfrontal; **pop**, paraoccipital process; **prf**, prefrontal; **ps**, parasphenoid; **pt**, pterygoid; **q**, quadrate; **qc**, quadrate condyle; **qj**, quadratojugal; **rn**, right nasal; **sa**, surangular; **st**, supratemporal; **sta**, path for the stapedial artery; **stp**, stapes; **tur**, tuberous ridge; **v**, vomer; **vc**, vertebral centrum; **vf**, vagus foramen. Scale bars: A-B = 50 mm; C-E, G-H = 20 mm; F = 10 mm.

Stapes: Only the right stapes is visible. It is located on the left side of the skull behind the basisphenoid and anterolateral to the displaced basioccipital, with its proximal head anteriorly oriented (Fig. 4B, 5G,). It is almost completely exposed in posteromedial view. The shaft of the stapes is straight and moderately thick (minimal diameter of the shaft to stapedial head height = 0.4), its length is approximately 1.5 the height of the proximal head (Fig. 5H). The stapedial proximal head is massive. The facet for the basioccipital is larger than that for the opisthotic. The angle between these two facets is approximately 120°. Ventral to the basioccipital facet, angled just over 90°, the facet for the pterygoid is well demarcated. On the distal border of the pterygoid facet, the path of the stapedial artery (following Moon & Kirton, 2016, fig. 15) is demarcated by a small protuberance (Fig. 5H). The ventral surface of the stapedial shaft is more concave than the dorsal one. The distal end of stapes has a large and slightly convex condyle for the articulation with the quadrate.

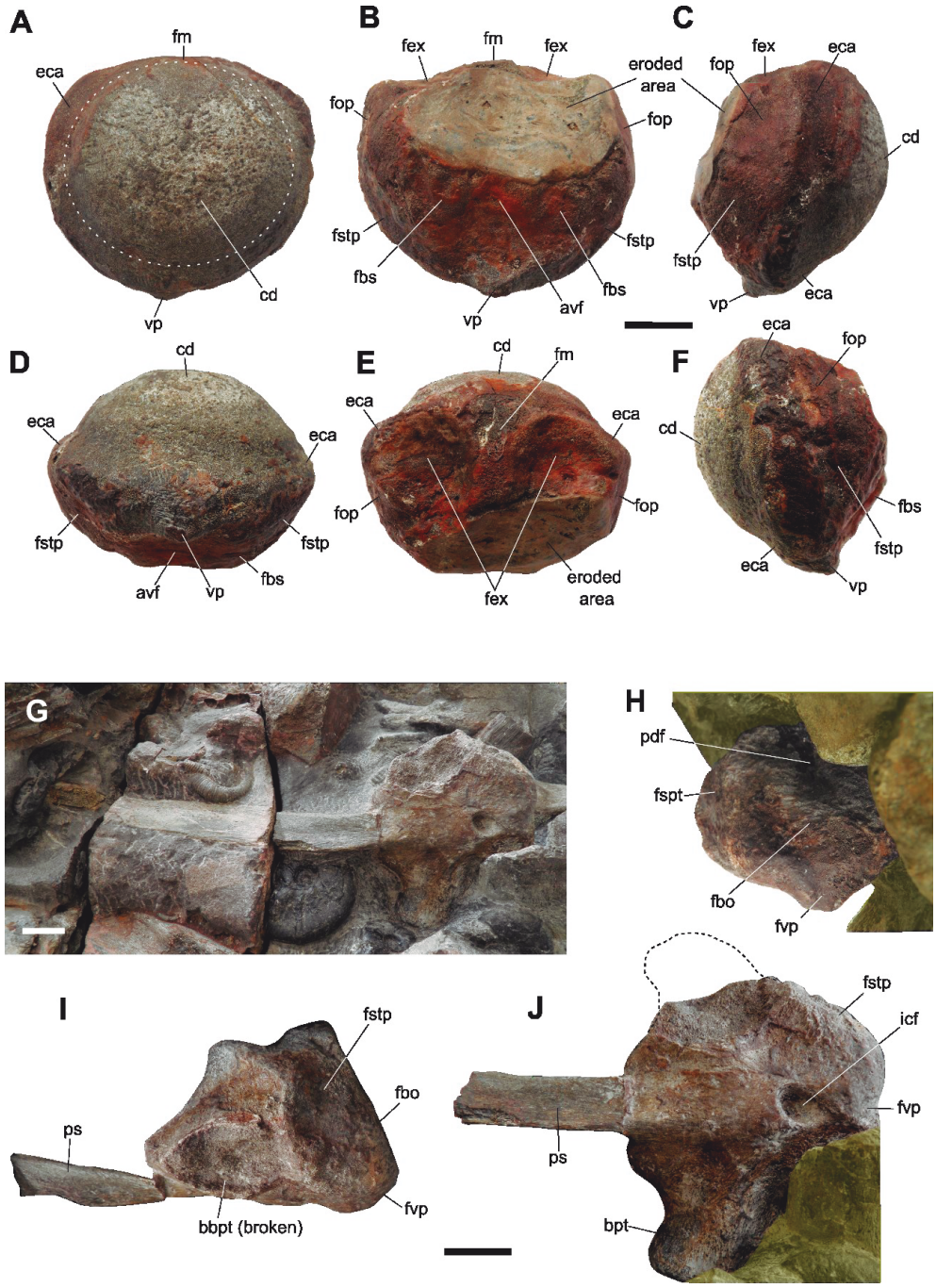

Figure 6. *Platypterygius elsuntuoso* sp. nov., holotype FCG-CBP-28. Basicranial elements. **A-F**, basioccipital in **A**, posterior, **B**, anterior, **C**, left lateral, **D**, ventral, **E**, dorsal and **F**, right lateral views (see 3D model in supplemental data 1). **G-J**, basisphenoid-parasphenoid in **G**, general, **H**, posterior, **I**, left lateral and **J**, ventral views. Yellow shading: all surfaces that do not belong to the illustrated bone. Abbreviations: **avf**, anteroventral fossa; **bbpt**, base of the basipterigoid process; **bpt**, basipterygoid process; **cd**, condyle; **eca**, extracondylar area; **fbo**, facet for the basioccipital; **fbs**, facet for the basisphenoid; **fex**, facet for the exoccipital; **fm**, foramen magnum floor; **fop**, facet for the opisthotic; **fstp**, facet for the stapes; **fvp**, facet for the basioccipital ventral peg; **icf**, internal carotid foramen; **pdf**, posterodorsal furrow; **ps**, parasphenoid; **vp**, ventral peg. Scale bars = 20 mm.

Palate

The palatal bones are only exhibited in cross-section on the natural fractures of the skull, or partly exposed on the left side of the skull (Fig. 4B; 5B). Most of the palatal bones are disarticulated, displaced from their anatomical position, and in some cases broken. Added to this is the fact that the left side of the skull is displaced forward relative to the right side, so there is no symmetry in the palatal bones when viewed in cross-section. Under these conditions, their recognition is difficult, and little can be described. At the orbital level, the palatine and the pterygoid can be seen forming a wide sheet 8 to 11 mm thick. Here, the palatine distally contacts the jugal and lacrimal, and the pterygoid medially thickens giving it a comma shape in cross-section.

Mandible

As the rostrum, the anterior part of the mandible is lost. The bones of the left ramus are disarticulated and displaced from their anatomical position, but the right ramus is well-preserved and provides a reliable description of the mandibular bones. This ramus is preserved from its posterior end to 33 cm anterior to the beginning of the symphysis.

Dentary. The dentary forms most of the lateral wall of the mandible (Fig. 4A). Its posterior end reaches the mid-length of the orbit, but the dental canal only reaches the level of the posterior region of the external naris. The dental canal is wide and shallow posteriorly and becomes deep anteriorly (Fig. 7D*b*-*e*). On the lateral surface the dentary bears a canal, which is narrow and deep anteriorly and slightly broadens and becomes shallower posteriorly at the same level as the lateral premaxillary canal broadens (Fig. 4A; 7D*c*-*e*).

Splenial. In ventral view and in the natural cross-sections of the specimen, the splenial can be seen in almost its complete length (Fig. 7D-*e*). It is the main component of the medial wall of the mandible. At the anterior end of the preserved portion of the mandible, the splenial is seen as a short vertical sheet that articulates with the ventral medial face of the dentary (Fig. 7D*e*). Just 10 cm anterior to the beginning of the symphysis, the splenial is seen in cross-section divided into two well-separated rami, indicating the presence of the anterior opening of Meckel's canal. Here, the dorsal portion of the splenial is very small and contacts the medial wall of the dental canal, and the ventral portion is larger and articulates with the ventral ramus of the dentary (Fig. 7D*d*). The greatest height of the splenial is found at the level of the posterior end of the symphysis, where it reaches the dorsal edge of the mandible forming the medial wall of the Meckelian canal (Fig. 7D*c*). At the level of the anterior orbit, the splenial becomes a narrow vertical lamina, ventrally curved enclosing the angular. It is exposed in ventral and lateral views to about the mid-orbit level (Fig. 4A). Medially, the splenial does not reach the dorsal edge of the mandible; it covers the angular and a small fraction of the prearticular (Fig. 7D*b*). The posterior end of the splenial is not visible in the specimen.

Angular. The angular is exposed on the lateroventral side of the mandible (Fig. 4A; 7A). In lateral view it extends between the surangular and the splenial from near the posterior end of the symphysis to the mid-orbit; then it forms the ventral portion of the posterior mandible. Externally, the anterior end of the angular contacts the dentary just for a few centimeters, just anterior to the anterior end of the surangular. Nevertheless, internally, the angular extends anteriorly in contact with the surangular to more than 10 cm in front of the beginning of the symphysis (Fig. 7D*d*). The angular is hardly exposed ventrally in the posteriormost symphysis. At the posterior region of the mandible the angular forms the total ventral edge of the mandible, and both medially and laterally it extends dorsally forming two walls. The lateral wall covers the surangular and the medial wall contacts laterally the prearticular. In the most posterior end, the medial wall of the angular is very thin; it is broken at its base and laterally displaced, but it can be seen that its dorsal edge thickens and bears a medial canal for the articulation with the prearticular (Fig. 7D*a*). In lateral view, the suture with the surangular is sinusoidal (Fig. 4A; 7A).

Surangular. The surangular is greater exposed than the angular in lateral view (Fig. 3A; 7A). Its externally exposed anterior end lies anterior to the anterior border of the external naris and posterior to the anterior tip of the maxilla (Fig. 4A). The distance between the exposed anterior end of the surangular and the anterior end of the maxilla in lateral view equals the length occupied by 6 maxillary teeth. Although in this region the surangular is little exposed laterally, internally it is robust, giving a solid support to the dentary and a thick lateral wall to the Meckelian canal (Fig. 7D*c*). The external anterior end of the surangular is placed more than 10 cm posterior to the beginning of the symphysis (Fig. 4A). At the level of the orbit, on the lateral surface, the surangular fossa is clearly demarcated (Fig. 7A). In the posterior margin, the fossa bears an oval foramen and behind this margin two more foramina are present. Posterior to the orbit, the dorsal edge of the surangular raises forming the anterior portion of the glenoid fossa, which faces dorsomedially for the articulation with the ventrolateral facet of the quadrate condyle. Behind the articulation with the quadrate the surangular articulates with the articular medially (Fig. 7D*a*). The retroarticular process of the mandible is horizontally directed, and its posterior border has a curved outline. Here, the lateral surface of the surangular is strongly wrinkled (Fig. 7A), suggesting that in this region a powerful muscular attachment was done.

Prearticular. The prearticular is poorly exposed; it can be seen in cross-sections, but also its most posterior portion is exposed in medial view (Fig. 4B; 7D*a*-*b*). At the level of the external naris, the prearticular is a small vertical lamella that contacts the internal dorsal surface of the splenial contributing to the medial wall of the Meckelian canal (Fig. 7D*b*). At the level of the anterior orbit, the prearticular rises and thickens forming the medial wall of the Meckelian canal. At the glenoid region, the prearticular becomes robust, dorsally contacts the articular and ventrally articulates with the angular (Fig. 7D*a*).

Articular. The right articular is slightly displaced dorsally from its anatomical position and is covered by the left one, which is displaced to the posterior end of the right mandible ramus and is well exposed for description (Fig. 7A). The articular forms the posterior medial wall of the mandible. It is a short and mediolaterally compressed bone shaped like a longitudinally bent board. The dorsal edge is narrower than the ventral, and the anterior face is broad. In medial and lateral views, the articular is subrectangular in outline, with a slightly curved posterior edge. The lateral face of the articular is concave and closely joins the surangular (Fig. 7C). The medial surface is convex in dorsoventral direction and concave in anteroposterior direction, producing a saddle-shaped surface, which is smooth in texture (Fig. 7B). A blunt tubercle projects from the posterior face of the bone onto the dorsal region of the medial surface. Anteriorly, the articular widens erecting a planar vertical articular facet for the quadrate (Fig. 7B, C). The surface of this facet, as well as that of the dorsal, ventral and posterior faces of the bone is porous, indicating the articular was surrounded by cartilage.

Hyoids

A fragment of a slightly curved rod-like bone found near the medial wall of the right mandibular ramus and exposed on the left side of the specimen, is interpreted as a portion of a hyoid, probably the right one (Fig. 4A, B; 9K). This fragment is 215 mm in length and oval in cross-section, with 27 mm major diameter and 9 mm minor diameter.

Teeth and dentition

On the right side of the skull all the teeth are preserved emplaced in their anatomical position (Fig. 8). There are maximum of 18 teeth in the maxilla in lateral view. The number of premaxillary teeth remains unknown since the snout is incomplete. The teeth are implanted into a common dental canal (aulacodont condition sensu Mazin, 1983). They are densely packed and tightly interlocked. The teeth of the upper and lower jaws are almost regularly intercalated in nearly the same plane. In the posterior region the upper teeth slightly occlude laterally over the lower teeth, but in the anterior preserved region the occlusion is inverted, with the lower teeth occluding laterally over the upper teeth. The teeth are oriented nearly perpendicular to the bony labial border, with few random variations due to taphonomical processes. The posteriormost teeth are maxillary teeth, with the last position located at the level of the anterior orbital margin. In contrast, the posteriormost dentary tooth is seen at the level of the external naris, where the dentary dental canal begins. The maxillary and premaxillary teeth are larger than their opposing dentaries. The posterior teeth on both maxilla and dentary are the dorsoventrally shortest teeth, which concurs with the posterior shallowing of the dental canals.

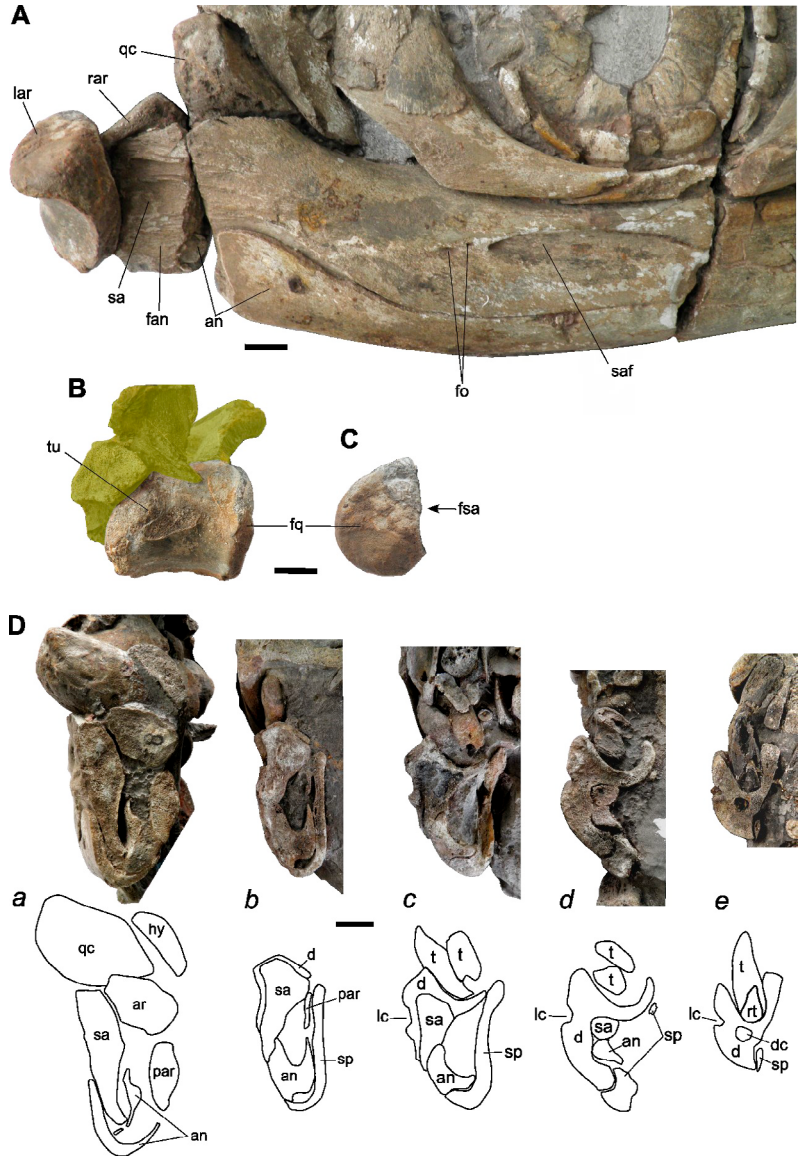

Figure 7. *Platypterygius elsuntuoso* sp. nov., holotype FCG-CBP-28. Mandible. **A**, posterior region of the right mandible in lateral view. **B-C**, left articular in **B**, medial and **C**, anterior views. **D**, cross-sections of the mandible as referred in Fig. 2A; the section *a* was inverted to illustrate the sequence of images in the same direction. Yellow shading: all surfaces that do not belong to the illustrated bone. Abbreviations: **an**, angular; **ar**, articular; **d**, dentary; **dc**, dentary canal; **fan**, facet for the angular; **fo**, foramen; **fq**, facet for the quadrate condyle; **fsa**, facet for the surangular; **hy**, hyoid; **lar**, left articular; **lc**, lateral canal; **par**, prearticular; **qc**, quadrate condyle; **rar**, right articular; **rt**, replacement teeth; **sa**, surangular; **saf**, surangular fossa; **sp**, splenial; **t**, tooth; **tu**, tubercle. Scale bars = 20 mm.

The functional teeth have a very tall root and a short, enameled crown (total tooth length/crown length ratio: 3.7) (Fig. 8F). There is a transition region of acellular cementum (sensu Maxwell et al., 2011), in which shallow grooves from the crown striae extend over a not enameled surface that differs in texture from the root (Fig. 8D, L). On both the upper and lower jaws, and along the entire length of the snout, the acellular cementum ring and nearly one-third of the root of the functional teeth are exposed outside the dental canal (Fig. 8F).

The root is subrectangular in cross-section, being longer labiolingually than mesiodistally (Fig. 8C, N). The root exhibits a slight neck at the base of the acellular cementum ring (Fig. 8F, O). In longitudinally broken teeth, the root exhibits a hollow center, as an extension of the crown pulp cavity (Fig. 8B). The external surface of the root bears slight grooves and shows a fibrous and porous texture indicating a high vascularization (Fig. 8F, L).

The enameled crown is conic, circular in cross-section, with the apex very slightly curved lingually. The crown is short, its height is 1.3 to 1.7 times its base length; shorter in the most posterior teeth. The base of the enamel is well defined (Fig. 8D-L). The enamel is ridged all around the crown. The ridges extend along the entire enamel height without bifurcations. They are thicker at the crown base and more densely packed at the apex. At the tip of the crown the ridges become discontinuous producing an apical grainy texture. This apical grainy texture is found in all well-preserved crowns, whether from upper or lower jaw teeth, anterior or posterior teeth, or replacement or functional teeth (Fig 8D-K).

The replacement teeth are found in different degrees of growth, from very immature teeth with only the crown apex exposed, to erupted teeth, in which the only difference from the mature ones is their slightly smaller size. The dental replacement occurs directly from the base of the root. In the longitudinal section of a dentary functional tooth located in the anterior end of the preserved snout, the base of the root is seen resorbed by the growth of a replacement tooth (Fig. 7D*e*). That differs from the lingual replacement described by Kear (2005) for *P. australis*. The just erupted replacement teeth show their crown in the center of the ejected tooth root (Fig. 8J). In the growth process, the crown is the first to be formed and, once it is emplaced into the alveolus, the tooth becomes functional progressively increasing the size of the root.

There are no regions with differentiated dentition on the preserved portion of the snout. Instead, when the teeth of the upper jaw are carefully observed, two intercalated growth waves can be identified, one on the even positions (white teeth in Fig. 8M) and the other on the odd positions (dark gray teeth in Fig. 8M). The alternate pattern in growth dentition in reptiles had already been described by Edmund as early as 1960. Edmund (1960) shows that a replacement occurring in alternate waves passing from front to back is a peculiarity of ichthyosaurs, differing from the usual back-to-front wave progression found in most reptiles.

As Edmund (1960) observed for Ichthyosauria, in the studied specimen the intercalated growth waves are done from front to back. From the first tooth position preserved on the upper jaw, a sequence of growth stages in odd positions is clearly observed reaching position 9, where a large hollowed broken out root indicates a just replaced tooth (Fig. 8M). The following upper odd positions show large functional teeth up to position 21. For the even positions, two waves of consecutive growth stages are clearly identified with the large functional teeth in positions 2 to 8 and 18 to 22 (Fig. 8M). In the posteriormost dentition all the maxillary teeth seem to be functional and do not have mandibular opposites.

The described replacement structure shows that within each series (odd and even), several replacement waves follow each other. Given the intercalation between the two series, the large functional teeth from one of the series intercalate with the smaller replacement teeth from the other (Fig. 8M). This replacement pattern ensures no gaps of more than one functional tooth in the upper jaw. It also generates multiple series of consecutive large teeth that in life changed their position repeatedly following the growth alternating waves. Under these conditions, to give interpretations on dentition regionalization or mode of feeding based on what was preserved in a fossil could be misleading.

Contrary to the upper jaw, a sequence of replacement teeth in the dentary is difficult to discern. Nevertheless, it is interesting to note that opposing each smaller replacement tooth on the upper jaw, there are usually two adjacent large functional teeth on dentary, and the smaller replacement dentary teeth are located where a series of consecutive functional teeth in the upper jaw is found (Fig. 8M). The number of dentary teeth is somewhat greater than that of their opposing in the upper jaw. In fact, thirty-one dentary teeth can be counted in the space containing the twenty-seven opposing positions of the upper jaw.

Postcranial axial elements

From the axial skeleton only a few anterior vertebral elements, including the atlas-axis-complex, and ribs fragments are preserved. These elements are found disarticulated in the posterodorsal region of the skull (Fig. 4).

Atlas-axis: The atlas-axis complex is incomplete; it is longitudinally broken and partially embedded in sediment. Only the anterior, posterior dorsal, right laterodorsal and left lateroventral portions can be seen (Fig. 9A, B). The atlas-axis complex was preserved behind the basioccipital but out of its anatomical position (Fig. 4). The atlas and the axis are fused, there is no suture between the two elements internally, as can be seen in the broken surface. However, a suture is clearly visible on the external surface. The atlas-axis complex is as high as it is wide (approximately 83 mm high and 84 mm wide) and its ventral length is greater than its dorsal length (approximately 59 vs. 51 mm) (Fig. 9 A, B). The identification of the atlas and axis was based on two criteria: The concavity of the atlas is circumscribed by a broad edge whereas the posterior concavity of the axis has a clearly demarcated edge as McGowan & Motani (2003) described as a criterion for the identification of the axis; the articular surface concavity of the atlas fits perfectly with the basioccipital condyle convexity, while that of the axis does not.

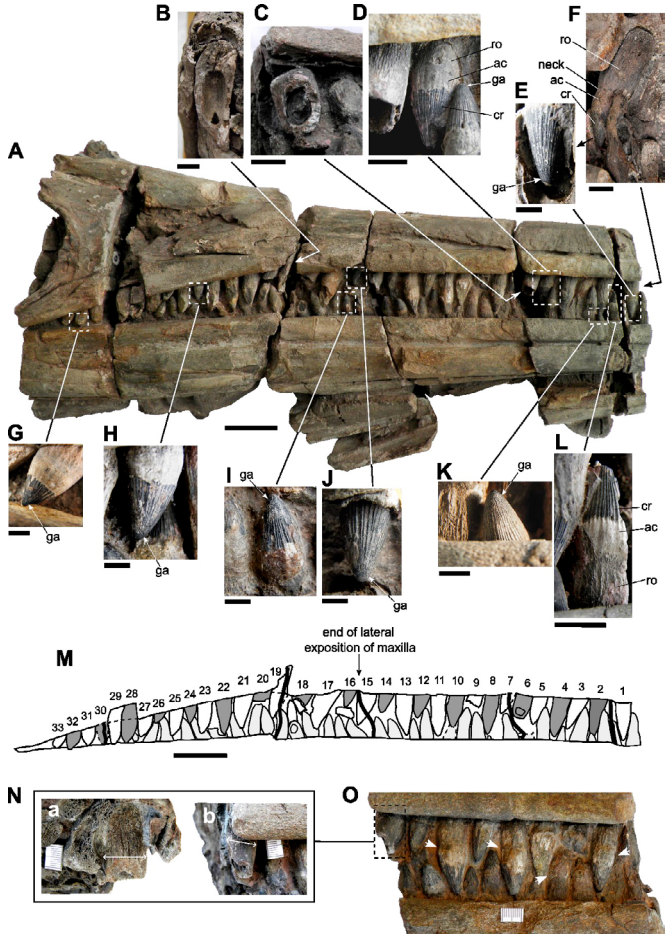

Figure 8. *Platypterygius elsuntuoso* sp. nov., holotype FCG-CBP-28. Dentition. **A**, general view of dentition. **B-L** details of teeth. **M**, scheme showing the growth pattern of replacement dentition with dentary teeth in light gray, dental positions of the upper jaw in dark gray (even positions) and white (odd positions); **N**, the same rectangular tooth root (indicated in O) from distal (a) and labial (b) views, showing the transverse side longer than the longitudinal side (double arrows). **O**, Detail of the dentition showing the neck at the base of the acellular cementum on teeth (white arrows). Abbreviations: **ac**, acellular cementum; **cr**, crown; **ga**, grainy apex; **ro**, root. Scale bars: **A**, **M** = 50 mm; **B-D**, **F**, **L** = 10 mm; **E**, **G-K** = 5 mm; **N-O** (mm).

The atlas centrum is slightly longer than the axis centrum (Fig. 9A). The right diapophyses and parapophyses are visible. In both atlas and axis, the diapophysis is close to the anterior edge of the centrum, united to the neural arch facet, whereas the parapophysis is placed near the posterior edge of the laterodorsal surface of the centrum. The diapophysis and parapophysis are closer to each other on the atlas than on the axis. The visible left lateroventral surface of the preserved portions of the atlas and axis are each demarcated by a depression. These depressions delimit the ventral facets for the atlantal and axial intercentra and apparently also a ventral crest (Fig. 9B).

Cervical vertebrae: Three complete and one incomplete anterior cervical centra and four neural arches and spines can be identified. All these elements are disarticulated; the neural arches are grouped near and inside the temporal fenestra and the centra are found posterior to them (Fig. 4). The centra are pentagonal in outline, slightly higher than wide (68 mm in height and 62 mm in width) (Fig. 9D). Their concave articular faces have a deeper central concavity. The diapophysis and parapophysis are separated in all centra, but the distance between them varies slightly. In all, the diapophysis is located close to the anterior edge of the centrum, united to the neural arch facet, but the parapophysis is found in different positions. In one of the centra, here considered a more anterior centrum, the parapophysis is near the posterior edge of the laterodorsal surface of the centrum, as in the axis. In the other two complete centra, the parapophysis appears at the middle length of the lateral surface of the centrum (Fig. 9E). The partially exposed neural arch shows long neural spines.

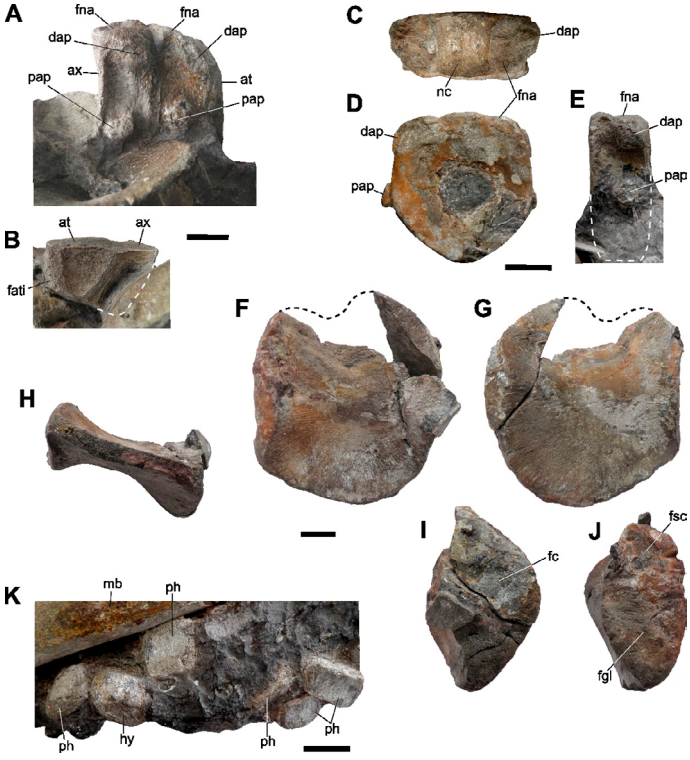

Figure 9. *Platypterygius elsuntuoso* sp. nov., holotype FCG-CBP-28. Postcranial elements. **A-B**, Atlas-axis complex (the preserved portion) in **A**, right lateral and **B**, left lateroventral views. **C-E**, cervical vertebra in **C**, dorsal, **D**, posterior and **E**, right lateral views. **F-J**, Left coracoid in **F**, dorsal, **G**, ventral, **H**, posterior, **I**, medial and **J**, lateral views. **K**, disarticulated phalanges in exposed view. Abbreviations: **at**, atlas; **ax**, axis; **dap**, diapophysis; **fati**, facet for the atlantal intercentrum; **fc**, intercoracoid facet; **fgl**, facet for the glenoid; **fna**, facet for the neural arch; **fsc**, facet for the scapula; **hy**, hyoid; **mb**, mandible; **nc**, neural canal floor; **pap**, parapophysis; **ph**, phalange. Scale bars: A-B = 20 mm; C-E = 20 mm; F-J = 20 mm; K = 20 mm.

Ribs: In the posterior dorsal region of the skull there are some fragments of an elongated element that could correspond to a broken rib (Fig. 4). These fragments are long and slender, with oval cross-section in the thicker fragments and circular in the thinner ones. These fragments show a central cavity, empty by erosion.

Appendicular elements

Coracoid: The left coracoid was found at the posterior end of the skull (Fig. 4) and was extracted during preparation. Its anterior region is damaged; therefore, the morphology of the anterolateral notch remains unknown (Fig. 9F, G). In dorsal or ventral view, the coracoid is nearly circular in outline (120 mm in mediolateral width and 127 mm in anteroposterior length); there is not a posterior notch. The dorsal and ventral surfaces are mediolaterally concave and anteroposteriorly convex, with a flattened posterior region 10 mm thick (Fig. 9F-H). The medial intercoracoidal facet is rhombic in outline and angled in such a way that in an anatomical position the body of the coracoid would be inclined approximately 15° to the horizontal plane (Fig. 9I). The medial facet is thicker (maximum thickness=58 mm) than the lateral (glenoid/scapular) facet (maximum thickness=48 mm). The lateral articular surface is oval in outline and shows a smaller anterior facet for the scapula and a greater posterior facet that contributed to the glenoid (Fig. 9J). The scapular facet is slightly dorsally directed, whereas the glenoid facet is laterally directed. Both the medial and lateral articular surfaces of the coracoid are pitted and rugous suggesting cartilage joints. The posterior border of the bone blade is notoriously porous (Fig. 9H), indicating a cartilaginous prolongation in this area.

Phalanges: Five disarticulated phalanges are preserved and partially exposed in the posterior ventral region of the skull (Fig. 4A, B; 9K). The largest are thick and rectangular in outline; the best exposed measures 30 mm x 20 mm x 14 mm. The smallest are thinner and suboval in outline (20-26 mm x 12-16 mm x 6-8 mm) and have less well-defined borders than the larger phalanges. The morphology of the preserved phalanges suggests that the smaller ones came from accessory digits while the larger ones, with their well-defined borders, were closely packed and occupied a more central position within the fin.

5. Discussion

FCG-CBP-28 is identified as *Platypterygius* by presenting the diagnostic features established for the genus: a skull with almost straight dorsal and ventral margins in lateral view; orbit proportionally small in comparison to the mandibular length (0.15-0.16); postorbital region proportionally extensive regarding the orbital length (0.45-0.60); external naris widely separated from the orbit and divided into an anterior and a posterior opening by a naso-maxillary pillar; quadratojugal with extensive lateral exposure, extracondylar area of the basioccipital reduced; tooth crown stout and having ridges along the entire enamel; coracoid with a poorly pronounced anteromedial process; and thick rectangular phalanges.

FCG-CBP-28 differs from all other *Platypterygius* species by having teeth with a neck at the base of the acellular cementum ring (Fig. 8F, O); in all other species such a neck is not present or has not been described (Broili, 1907; Cortés et al., 2021; Fischer, 2012; Fischer et al., 2014c; Kear, 2005; Kolb & Sander, 2009; Kuhn, 1946; Maxwell et al., 2019; Maxwell & Kear, 2010; Páramo, 1997). The basioccipital of FCG-CBP-28 bears a small anteroventrally directed peg in the ventral border of extracondylar area that fits into a posteroventral depression found in the basisphenoid, differing from that of *P. platydactylus*, *P. hercynicus*, *P. australis*, and *P. birjukovi* in which such a peg is not present (Broili, 1907; Fischer et al., 2014c; Kear, 2005; Kolb & Sander, 2009; Kuhn, 1946); this region of the basioccipital is unknown in *P. sachicarum* and *P. americanus* (Maxwell et al., 2019; Romer, 1968). The quadrate of FCG-CBP-28 has a supratemporal groove in the posterodorsal region (Fig. 5E) which is not present in *P. platydactylus*, *P. hercynicus*, and *P. australis* (Broili, 1907; Kear, 2005; Kolb & Sander, 2009; Kuhn, 1946); this quadrate region is unknown in the remaining species of *Platypterygius* (Cortés et al., 2021; Fischer et al., 2014c; Maxwell et al., 2019; Romer, 1968). In FCG-CBP-28 the basipterygoid processes of the basisphenoid are longer than in *P. platydactylus* and *P. australis* (Broili, 1907; Kear, 2005) and remains unknown in other species of *Platypterygius* (Cortés et al., 2021; Fischer et al., 2014c; Kear, 2005; Kolb & Sander, 2009; Kuhn, 1946; Maxwell et al., 2019; Romer, 1968). In addition to the noted particularities, FCG-CBP-28 exhibits the following features that differ from each species of *Platypterygius*.

The greatest morphological similarity is found with *P. sachicarum*. Two specimens have been assigned to *P. sachicarum*: the holotype skull (DON-19671) and a nearly complete skeleton (CIP-GA-01042014) preserving skull, presacral vertebral column, pectoral girdle, and partial forelimb (Cortés et al., 2021; Maxwell et al., 2019; Páramo, 1997). Photographs and a drawing taken in

1997 (ME P-F) show that some regions of the holotype of *P. sachicarum* were more complete at that time (e.g., orbit and maxilla) (Fig. 10) than at present (Cortés et al., 2021, fig. 2). On this basis, we could confirm that, in addition to the shared features noted by Maxwell et al. (2019), in both specimens the anterior external end of the maxilla is located at 2 times the orbital length from the anterior orbital margin, and the minimum number of maxillary teeth (or dental spaces) is 22-24 (personal observations). These features differ from other species of *Platypterygius* and support the assignment of both specimens to the same species *P. sachicarum*.

FCG-CBP-28 is slightly larger than specimens referred to *P. sachicarum* (Maxwell et al., 2019; Páramo, 1997) (Fig. 10). The morphology of the postorbital, supratemporal and quadratojugal of FCG-CBP-28 is comparable to that of *P. sachicarum*, as illustrated and interpreted by Páramo (1997), but not to that illustrated by Cortés et al. (2021, fig. 2B) (see Fig. 4A; 5A). The crown apex with a rugose texture on teeth along the dentition and the acellular cementum ring with shallow grooves found in FCG-CBP-28 is shared only with *P. sachicarum*; in the remaining species of *Platypterygius* the crown apex and the acellular cementum ring are smooth (Broili, 1907; Fischer, 2012; Kear, 2005; Maxwell & Kear, 2010). Cortés et al. (2021) stated that in the holotype of *P. sachicarum* the acellular cementum ring is smooth, and the crown apical rugose texture is present in teeth from one of their proposed dentition regions. However, our observations on the holotype of *P. sachicarum* revealed the presence of shallow grooves in the acellular cementum ring (Fig. 10A) and rugose apical texture on teeth from diverse positions of the preserved dentition (Fig. 10A-B). We also noted that no dentition regions are seen on the right side of the skull (Fig. 10A).

Despite the noted similarities, some differences between FCG-CBP-28 and *P. sachicarum* can be observed. The anterior external extension of the maxilla in *P. sachicarum* is proportionally longer than in FCG-CBP-28; its anterior end is located at 2 times the orbital length from the anterior orbital margin, whereas in FCG-CBP-28 it is located at 1.67 times the orbital length (Fig. 10). The externally exposed maxilla in *P. sachicarum* has 22-24 teeth (or dental positions) and probably reached 26 (Fig. 10), whereas in FCG-CBP-28 the maxilla bears 18 teeth. Moreover, the number of maxillary teeth counted between the anterior end of the surangular and the anterior end of the maxilla is 10-11 in the holotype of *P. sachicarum* and 5-6 in FCG-CBP-28. The teeth crowns in FCG-CBP-28 are proportionally shorter than in *P. sachicarum*; the ratio between the total tooth length and the crown length is 3 to 3.7 in FCG-CBP-28 and 2.6 to 3 in *P. sachicarum*. In both the holotype of *P. sachicarum* and FCG-CBP-28, the tooth root is rectangular in cross-section; however, in *P. sachicarum* the longer side is parallel to the dental canal, whereas in FCG-CBP-28 the longer side is transverse to the dental canal (Fig. 8N). We cannot be sure if this trait is present in other species of *Platypterygius* since the teeth roots are not frequently visible in both directions when the teeth are emplaced in the dental canal.

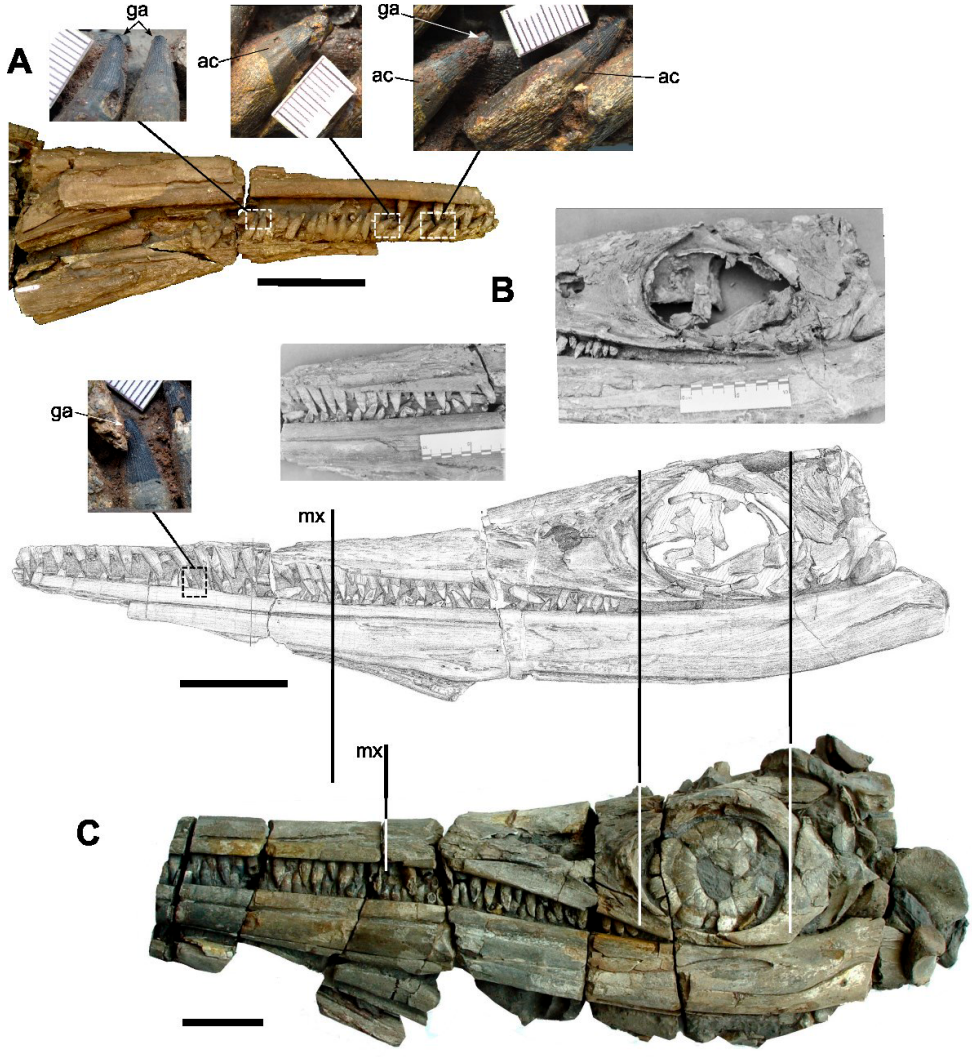

Figure 10. Comparison between the skull of *P. sachicarum* and *P. elsuntuoso*. **A-B**, holotype of *P. sachicarum* (DON-19671); **A**, photograph of the right-side dentition detailing some teeth; **B**, photographs and drawing taken in 1997 (ME P-F) with a recent photograph detailing a tooth. **C**, Photograph of the holotype of *P. elsuntuoso* (FCG-CBP-28) inverted to facilitate comparison. Both specimens were taken at the same orbital length to compare proportions. Note the difference in the external length of the maxilla (vertical lines) and in the number of maxillary teeth. Abbreviations: **ac**, acellular cementum; **ga**, grainy apex. Scale bars = 10 cm; teeth details (mm).

The differences noted between FCG-CBP-28 and *P. sachicarum* imply at least a slight specialization in diet, which supports a taxonomic distinction at the species level. The new species, named *P. elsuntuoso*, came from the lower Barremian and *P. sachicarum* came from the upper Barremian (Benavides-Cabra et al., 2023), so these differences may well represent speciation by adaptation to new food sources in the Cretaceous transgressional sea of Colombia. In this context, it is interesting to note that the forelimbs identified by Cortés & Páramo-Fonseca (2018) as *Platypterygius* sp. (specimen FCG-CBP-87) came from the same geographic locality and stratigraphic level as the holotype and only known specimen of *P. elsuntuoso*. Maxwell et al. (2019) noted morphological differences at the species level between the forelimb of FCG-CBP-87 and the forelimb of the specimen CIP-GA-01042014 of *P. sachicarum* (for details see Maxwell et al., 2019). Under these conditions, specimen FCG-CBP-87 could represent the forelimb of *P. elsuntuoso*. However, until a more complete specimen of *P. elsuntuoso* preserving both skull and forelimb is found, this hypothesis cannot be confirmed.

In addition to the features already mentioned, *P. elsuntuoso* differs from *P. platydactylus* in its long stapedial process, which is shorter in *P. playdactylus* and in the externally visible atlas-axis suture, which is not present in *P. platydactylus* (Broili, 1907, Taf. XIII-2, 3). From *P. hercynicus* it differs as follows: The posteroventral margin of the jugal has a marked angle in FCG-CBP-28 whereas in *P. hercynicus* is regularly curved (Kolb & Sander, 2009); the anterolateral process of the supratemporal is shorter in *P. hercynicus* (Fischer, 2012, fig. 2); in the basioccipital, the convexity of the condyle is less protruded in *P. elsuntuoso* than in *P. hercynicus* and the opisthotic facet is more dorsally and anteriorly directed in *P. hercynicus* than in *P. elsuntuoso* (for comparisons see Kuhn, 1946, Taf. II-2 and Taf. III-1a, b); the quadratojugal is less exposed laterally in *P. hercynicus* than in *P. elsuntuoso* (Fischer, 2012). From *P. birjukovi,* FCG-CBP-28 differs in the following features: The subnarial process of the premaxilla does not reach the posterior margin of the posterior narial opening as it does in *P. birjukovi* (Fischer et al., 2014c); the lateral premaxillary canal does not reach the external naris, differing from *P. birjukovi* where the canal reaches the anterior margin of the external naris (Fischer et al., 2014c); the extracondylar area is slightly exposed laterally and ventrally to the condyle, whereas in *P. birjukovi* the extracondylar area is practically not exposed (Fischer et al., 2014c); and the exoccipital facets of the basioccipital are more separated from each other than in *P. birjukovi* (Fischer et al., 2014c).

P. elsuntuoso differs from *P. americanus* in the additional following features. In *P. elsuntuoso* the supranarial process of the premaxilla is shorter than in *P. americanus* (Romer, 1968). The lateral premaxillary canal in *P. elsuntuoso* does not reach the external naris, differing from *P. americanus* where the canal reaches the anterior margin of the external naris (based on photographs of the specimen UW 2421). The anterior extension of the maxilla in *P. americanus* is proportionally longer than in *P. elsuntuoso*; its anterior end is located at 2.5-2.6 times the orbital length from the anterior orbital margin (based and photographs of the specimen UW 2421), whereas in *P. elsuntuoso* it is located at 1.67 times the orbital length. FCG-CBP-28 has 18 teeth (or dental spaces) in the external exposed maxilla whereas *P. americanus* has 21 (based on photographs of the specimen UW 2421). The number of maxillary teeth counted between the anterior end of surangular and the anterior end of the maxilla is 10-11 in *P. americanus* (based on photographs of the specimen UW 2421) and 5-6 in *P. elsuntuoso*. In *P. elsuntuoso* the jugal forms approximately one quarter of the posterior orbital margin, unlike in *P. americanus* where the jugal does not participate in the posterior orbital margin (Romer, 1968). The supratemporal contacts the postorbital in *P. elsuntuoso* whereas in *P. americanus* does not (Romer, 1968). The angular-surangular external suture is sinuous in *P. elsuntuoso*, whereas in *P. americanus* it is more rectilinear (Romer, 1968). The atlas-axis suture is present externally in FCG-CBP-28 whereas in *P. americanus* it is not (Maxwell & Kear, 2010).

The highest number of differences are found with *P. australis*. The anterior extension of the maxilla in *P. australis* is proportionally shorter than in *P. elsuntuoso*; its anterior end is located at a distance equivalent to one orbital length from the anterior orbital margin (Kear, 2005, fig. 1), whereas in *P. elsuntuoso* it is located at 1.67 times the orbital length. *P. elsuntuoso* has 18 teeth in the external exposed maxilla whereas *P. australis* has 26 (Kear, 2005; Wade, 1984; 1990). The number of maxillary teeth counted between the anterior end of the surangular and the anterior end of the maxilla is 8-9 in *P. australis* (based on photographs of the specimen QM F2453) and 5-6 in *P. elsuntuoso* (Fig. 4A). The surangular is proportionally longer than the angular in *P. australis* than in *P. elsuntuoso*, since the number of maxillary teeth counted between the anterior end of the angular and the anterior end of the surangular is 5-6 in *P. australis* (based on photographs of the specimen QM F2453) whereas it is 2 in *P. elsuntuoso* (Fig. 4A). In *P. elsuntuoso* the lacrimal forms the posterior margin of the external narial opening, differing from *P. australis* where the maxilla has a posterodorsal process excluding the lacrimal from the narial margin (Kear, 2005). The nasal has a wing above the external naris in *P. australis* (Kear, 2005), which is absent in *P. elsuntuoso*. In *P. elsuntuoso* the jugal is anteriorly short, just surpassing the anterior orbital margin (Fig. 4A), whereas in *P. australis* the anterior end of the jugal reaches the anterior end of the lacrimal (Kear, 2005). In *P. elsuntuoso* the pineal foramen is surrounded by processes of the frontal, whereas in *P. australis* the pineal foramen is surrounded by the parietal and frontals almost in the same proportions (Kear, 2005); The anterolateral process of the supratemporal is longer in *P. elsuntuoso* than in *P. australis* (Kear, 2005). In the basioccipital, the extracondylar area is exposed laterally and ventrally to the condyle in *P. elsuntuoso* (Fig. 6), whereas in *P. australis* is nearly absent (Kear, 2005); the exoccipital facets of the basioccipital are medially far from each other in *P. elsuntuoso* than in *P. australis* where these facets are medially close together (Kear, 2005) and the opisthotic facet is more dorsally and anteriorly directed in *P. australis* than in *P. elsuntuoso* (for comparisons see Kear, 2005, fig. 10 B, C). The stapes is longer in *P. elsuntuoso* than in *P. australis* (Kear, 2005). Lastly, in FCG-CBP-28 the atlas-axis suture is visible externally whereas in *P. australis* it is only visible on the dorsal surface (Zammit et al., 2010).

Phylogenetic analysis

The strict consensus of 708 most parsimonious trees with 589 steps (RI= 0.549 and CI= 0.292) obtained from TBR branch swapping, shows *Platypterygius elsuntuoso* within a large polytomy that includes all other *Platypterygius* species, *Plutoniosaurus bedengensis*, *Pervushovisaurus bannovkensis*, *Acuetzpalin carranzai*, *Sisteronia seeleyi*, and the other Colombian specimens: FCG-CBP-87 and CIP-GA-01042014. After applying the IterPCR algorithm, 4 unstable OUTs were identified: *Brachypterygius extremus*, *Pervushovisaurus bannovkensis* and the Colombian specimens FCG-CBP-87 and CIP-GA-01042014. After pruning the unstable OUTs from the consensus, the reduced strict consensus (Fig. 11) shows *Platypterygius elsuntuoso* as the sister taxon of *P. sachicarum* highlighting again their resemblance. This node is supported by the presence of vertical grooves basal to the crown and apical to the root osteocementum [4.0]. The node containing *P. elsuntuoso* and *P. sachicarum* is recovered as sister taxon of *P. hercynicus* and *P. platydactylus* in a branch together with all the other *Platypterygius* species (including *P. birjukovi*), "*Plutoniosaurus*" *bedengensis*, and *Sisteronia seeleyi*. This branch is supported by an atlas-axis with a ventral keel [78.1].

According to what was discussed above, the known material of "*Simbirskiasaurus*" *birjukovi* falls within the morphology characterizing *Platypterygius* representing a species of *Platypterygius* instead of a separated genus, thus its location together within the *Platypterygius* branch was expected and support its inclusion withing the genus *Platypterygius*. Even though the original description of "*Plutoniosaurus*" *bedengensis* (Efimov, 1997) did not offer many details, Zverkov & Efimov (2019) provided the scoring of the holotype specimen based on their personal observations (extended by Zverkov & Jacobs, 2021). Based on that scoring, "*Pl.*" *bedengensis* is recovered here together with all the *Platypterygius*. We interpret that this specimen probably represents a species within *Platypterygius*, however, until a formal reevaluation of the species is made available, we refrain to reassign it to *Platypterygius*. *Sisteronia seeleyi* is known only by fragmentary material of which the occipital region elements resemble with minor differences those known from *Platypterygius*, However, *S. seeleyi* also differs from *Platypterygius* in the humerus morphology and in the teeth morphology. We interpret that although *Sisteronia* appears to be a separated genus, its fragmentary material does not allow a clear differentiation with *Platypterygius* in the phylogenetic analysis.

The *Platypterygius* branch is contained within a clearly separated clade (A) (see Fig. 11) that also includes *Athabascasaurus bitumineus*, *Parrassaurus yacahuitztli*, *Otschevia alekseevi*, *Caypullisaurus bonapartei*, *Acuetzpalin carranzai*. This clade is supported by the following synapomorphies: long

premaxillary process of the maxilla [13.0]; nasal lacking a posterior process that overlaps the postfrontal dorsally [34.1]; square squamosal [47.0]; and extensive quadratojugal exposure [48.0].

The sister clade of (A) is clade (B). Clade (B) is composed by the *Nannopterygius* species, *Thalassodraco etchesi*, *Maiaspondylus lindoei*, *Sveltonectes insolitus*, *Aegirosaurus leptospondylus* and the other Colombian taxon *Muiscasaurus catheti*. The position of *M. catheti* differs from that recovered in previous phylogenetic analysis (Barrientos-Lara & Alvarado-Ortega, 2021a; 2021b; Maxwell et al., 2016; 2019; Páramo-Fonseca et al., 2021; and others) in which *M. catheti* was recovered closely related to *Ophthalmosaurus* or to *Platypterygius*. The clade (B) is supported by the following synapomorphies: snout depth very short [7.0]; external nares elongated and complex lobated [15.1]; prefrontal having a processus narialis [21.1]; lower jaw ventral margin markedly concave [72.1]; and rib facet in anterodorsal centra confluent with anterior face, at least in some centra [84.0].

Two other well separated clades, (C) and (D), were recovered within Ophthalmosauridae (see Fig. 11). Clade (C) includes the *Undorosaurus* species, *Jabalisaurus meztli*, *Acamptonectes densus*, *Catutosaurus gaspariniae,* and *Sumpalla argentina*. This clade is supported by a descending process of the nasal almost completely dividing the naris [17.2]; a robust supratemporal process of the parietal [43.1]; an interclavicle markedly expanded [99.1]; protruding triangular deltopectal crest [104.1]; and an intermedium proximal edge straight or notched [123.0]. Clade (D) is composed of the *Ophthalmosaurus* species and *Gengasaurus nicosiai* and is supported by a basioccipital condyle with a peripheral lateral and ventral groove [56.1] and by an elongated and slender paraoccipital process of the opisthotic [66.1].

Our analysis also recovered a monophyletic link for the *Undorosaurus* species and for the *Arthropterygius* species, as was recovered in other recent analysis (see Jacobs & Martill, 2020; Páramo-Fonseca et al., 2021; Zverkov & Jacobs, 2021; Zverkov & Prilepskaya, 2019). *Undorosaurus* is supported by the presence of deep longitudinal ridges on the crown [1.0]; root with a quadrangular cross-section [3.1]; stapedial shaft moderately thick in posterior view [67.0]; and short surangular in lateral view, not surpassing the level of the external naris midlength [145.1]. *Arthropterygius* is supported by a processus subnarialis of the premaxilla that reaches the posterior end of the naris [10.1]; presence of a processus narialis of the prefrontal [21.1]; posterior margin of the jugal excluded from the quadratojugal by the postorbital [28.1]; anteroposteriorly short parietal medial symphysis [41.1]; squamosal absent [47.2]; basisphenoid processes short and anteriorly directed [52.0]; internal carotid foramen located in the posterior surface of the basisphenoid [53.2]; presence of a raised opisthotic facet for the basioccipital [62.1]; osseous labyrinth T-shaped [65.1]; tail fin centra as wide as they are high [82.1]; angle between the articulated coracoids below 130º [94.2]; absence of a protruding triangular deltopectoral crest on humerus [103.0]; wide distal femoral blade absent [138.1].

Clades (A) and (B) form a more inclusive clade (E), and clades (C) and (D) with *Arthropterygius* spp., *Leninia stellans* and *Mollesaurus perialus* form a more inclusive clade (F). Both, clade (E) and (F) represent Ophthalmosauridae. Our results show that the topology and composition of the different clades proposed within Ophthalmosauridae is highly variable (Barrientos-Lara & Alvarado-Ortega, 2021a; 2021b; Campos et al., 2021; Cortés et al., 2021; Delsett et al., 2019; Fernández et al., 2021; Zverkov, 2022; and this work), indicating that the phylogenetic relationships within Ophthalmosauridae are far from being completely resolved and understood. Under these conditions, in this work we refrain to name and define the different clades recovered within Ophthalmosauridae in our phylogenetic analysis.

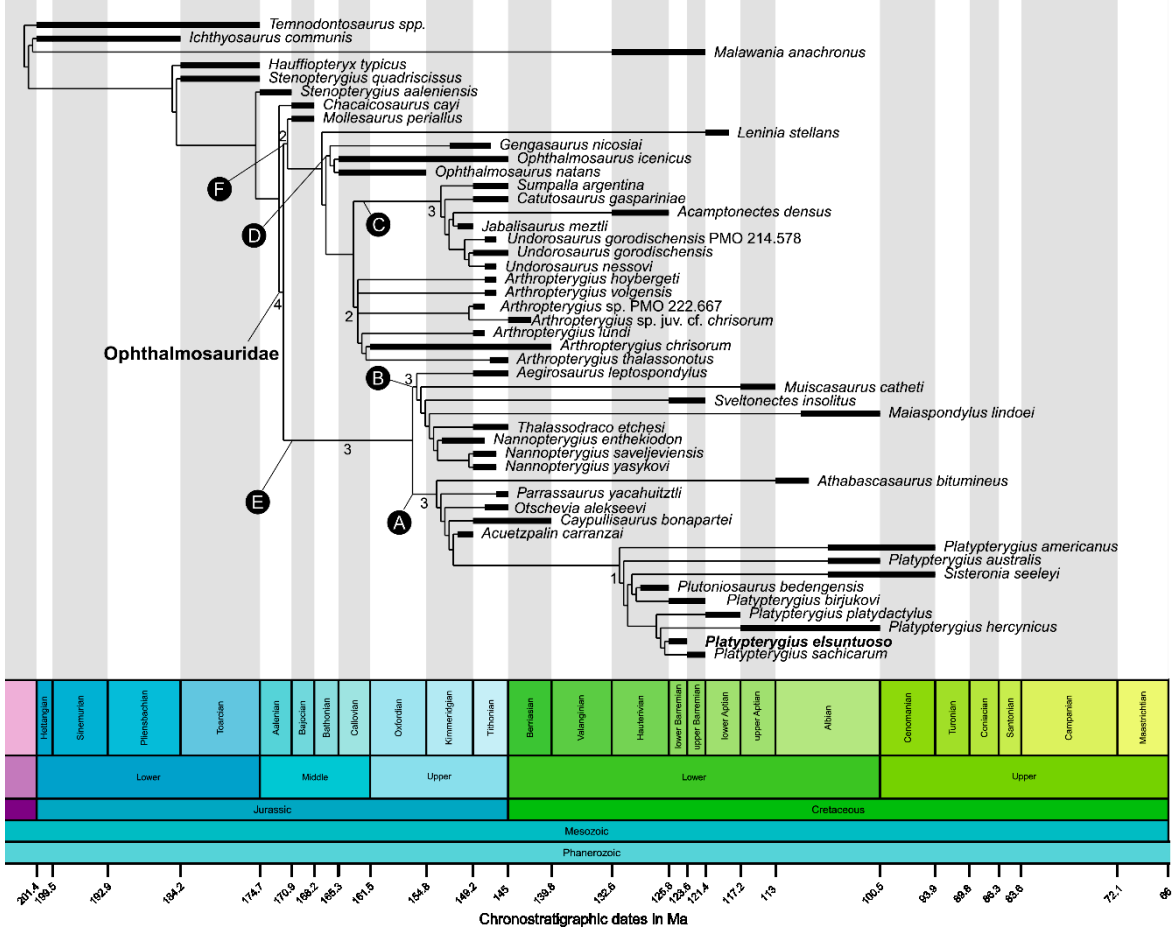

Figure 11. Phylogeny of Ophthalmosauridae showing the position of *Platypterygius elsuntuoso* sp. nov. Time calibrated strict reduced consensus from 708 most parsimonious trees (589 steps) with 52 OTUs and 145 characters (see Materials and Methods) recovered from the analysis of the full dataset. Bremer support values are shown in some branches. The letters within a black circle **(A)-(F)** indicate the different identified clades.

Conclusions

Our evaluation of the genus *Platypterygius* showed that this genus is distinguished from all other ophthalmosaurids from cranial and appendicular features. The forelimb of the type species *P. platydactylus* and those of *P. americanus*, *P. australis*, *P. hercynicus*, and *P. sachicarum* share a combination of features not found in other ophthalmosaurids. Among these features, the following were found to be exclusive to the genus: The distally oriented articular facets for the ulna and the radius on the humerus; the roughly pentagonal shape of the intermedium with parallel anterior and posterior sides and longer and straight distal side; and the relations of the intermedium with surrounding elements, fitting between the radius and ulna and contacting almost exclusively radiale, ulnare and distal carpal 3.

Based on the morphology of the specimens of *Platypterygius* preserving both cranial and forelimb remains, we found that the skull of this genus is characterized and differentiated from the other Cretaceous ophthalmosaurids by a combination of characters that include a large size (surpassing 70 cm in length), a skull with almost straight dorsal and ventral margins in lateral view, a proportionally small orbit relative to the mandible length, an extensive postorbital region, and an external naris divided in two openings by a naso-maxillary pillar, among others. Since the morphology of the forelimb and skull of *P. sachicarum* concur with that of *Platypterygius*, the recently erected name "*Kyhytysuka*" proposed to differentiate *P. sachicarum* is here rejected. In addition, given that the morphology of "*Simbirskiasaurus*" concurs with that found in *Platypterygius*, we found not sufficient evidence to support a generic differentiation of this taxon. Therefore, we consider these two names to be junior synonyms of *Platypterygius*.

The morphology of the new specimen here described, concurs with the diagnostic features of the genus *Platypterygius*, supporting its inclusion in this genus. The differences noted between the new specimen and all other *Platypterygius* species, support the erection of a new species, *P. elsuntuoso*. Among a particular combination of characters defining the new species, three unique features among *Platypterygius* were recognized: 1- The anterior ventral border of the extracondylar area of the basioccipital bears a small ventral peg anteroventrally directed, which fits into a posteroventral depression found in the basisphenoid; 2- Quadrate with supratemporal groove dorsal to the stapedial foramen; and 3- Root of teeth with a shallow neck at the base of the acellular cementum ring.

The morphological comparisons and our phylogenetic analysis show *P. elsuntuoso* more closely related to *P. sachicarum* than to other *Platypterygius* species. The phylogenetic analysis recovered all the *Platypterygius* species in a single clade together with *Plutoniosaurus* and *Sisteronia*. However, the different branches recovered within Ophthalmosauridae are still not well-supported indicating that the phylogenetic relationship between the ophthalmosaurids is not yet entirely understood.

We concluded that *Platypterygius* is a genus distinguished by a characteristic forelimb structure and a particular combination of skull features. We emended its diagnosis and recognized as valid the Barremian to lower Cenomanian species *P. platydactylus*, *P. americanus*, *P. australis*, *P. hercynicus*, *P. sachicarum*, *P. birjukovi* and the new species *P. elsuntuoso*. Thus, *Platypterygius* was a cosmopolitan genus that diversified as it conquered the waters of the Early to early Late Cretaceous oceans and seas.

Acknowledgments

We especially want to thank the Padilla brothers, Carlos Bernardo and Santiago (Founders of the CIP) who, before passing away, allowed us to study the specimen; we dedicate this work to their memory. We are grateful to Dr. Fernando Etayo-Serna for his comments on the ammonoid taxonomy and biostratigraphic context. We extend our thanks to Mary Luz Parra-Ruge, Juan de Dios Parra-Ruge and Fredy Parra-Ruge from the CIP for the excellent preparation of the fossil. We also thank Mary Luz Parra-Ruge for allowing us to review the specimens of *Platypterygius* housed in the CIP. Furthermore, we are grateful to the CIP staff for all their patient support during our study visits. Likewise, we are grateful to H. D. Palma from Departamento de Biología of the Universidad Nacional de Colombia for producing the 3D model of the basioccipital. We thank Victoria Corredor from the Museo José Royo y Gómez of the SGC for allowing us to review the holotype of *P. sachicarum*. We also thank Jamie MacLaren and Valentin Fischer for providing useful photos of *P. americanus* and *P. australis* that were used in our comparisons. We are grateful to Nikolay Zverkov and an anonymous reviewer for their constructive comments, which helped to improve the current version of the manuscript.

Supplemental information

Supplemental Data 1: Textured and scaled 3D model of basioccipital (https://doi.org/10.6084/m9.figshare.24434182)

Supplemental Data 2: Character scoring

Supplemental Data 3: Data matrix

References

Appleby, R. M. (1956). The Osteology and Taxonomy of the Fossil Reptile *Ophthalmosaurus*. *Proceedings of the Zoological Society of London*, 126(3), 403-448. https://doi.org/10.1111/j.1096-3642.1956.tb00447.x

Arkhangelsky, M. S. (1998). On the Ichthyosaurian Genus *Platypterygius*. *Paleontological Journal, 32*.

Arkhangelsky, M. S., Averianov, A. O., Pervushov, E. M., Ratnikov, V. Y., & Zozyrev, N. Y. (2008). On ichthyosaur remains from the Cretaceous of the Voronezh Region. *Paleontological Journal,* 42(3), 287-291. https://doi.org/10.1134/S0031030108030106

Bapst, D. W. (2012). Paleotree: An R package for paleontological and phylogenetic analyses of evolution. *Methods in Ecology and Evolution*, 3(5), 803-807. https://doi.org/10.1111/j.2041-210X.2012.00223.x

Bardet, N. (1989). Un crâne d'Ichthyopterygia dans le Cénomanien du Boulonnais. *Mémoires de La Société Académique Du Boulonnais*, 6(1), 1-32.

Bardet, N., & Fernández, M. S. (2000). A new ichthyosaur from the Upper Jurassic lithographic limestones of Bavaria. *Journal of Paleontology,* 74(3), 503-511. https://doi.org/10.1666/0022-3360(2000)074<0503:ANIFTU>2.0.CO;2

Barrientos-Lara, J. I., & Alvarado-Ortega, J. (2020). *Acuetzpalin carranzai* gen et sp. nov. A new ophthalmosauridae (Ichthyosauria) from the Upper Jurassic of Durango, North Mexico. *Journal of South American Earth Sciences,* 98, 102456. https://doi.org/10.1016/j.jsames.2019.102456

Barrientos-Lara, J. I., & Alvarado-Ortega, J. (2021a). A new ophthalmosaurid (Ichthyosauria) from the Upper Kimmeridgian deposits of the La Casita Formation, near Gómez Farías, Coahuila, northern Mexico. *Journal of South American Earth Sciences,* 111, 103499. https://doi.org/10.1016/j.jsames.2021.103499

Barrientos-Lara, J. I., & Alvarado-Ortega, J. (2021b). A new Tithonian ophthalmosaurid ichthyosaur from Coahuila in northeastern Mexico. *Alcheringa: An Australasian Journal of Palaeontology,* 45(2), 203-216. https://doi.org/10.1080/03115518.2021.1922755

Baur, G. (1887). Über den Ursprung der Extremitäten der Ichthyopterygia. *Jahresberichte Und Mitteilungen Des Oberrheinischen Geologischen Vereines*, 20, 17-20.

Bell, M. A., & Lloyd, G. T. (2015). Strap: An R package for plotting phylogenies against stratigraphy and assessing their stratigraphic congruence. *Palaeontology,* 58(2), 379-389. https://doi.org/10.1111/pala.12142

Benavides-Cabra, C. D., Páramo-Fonseca, M. E., Palma-Castro, H. D., Narváez-Rincón, J. A., & Ramos-Clavijo, M. P. (2023). Stratigraphic distribution of marine vertebrates of the Arcillolitas abigarradas Member (Paja Formation) from the Villa de Leiva—Sáchica—Sutamarchán region, Boyacá, Colombia. *Earth Sciences Research Journal,* 27(3), 211-226. https://doi.org/10.15446/esrj.v27n3.108292

Blainville, H. D. (1835). Description de quelques espèces de reptiles de la Californie: Précédée de l'analyse d'un systéme général d'erpétologie et d'amphibiologie. *Nouvelles Annales Du Museum National d'Histoire Naturelle, Paris,* 4, 233-296.

Bremer, K. (1994). Branch Support and Tree Stability. *Cladistics,* 10(3), 295-304. https://doi.org/10.1111/j.1096-0031.1994.tb00179.x

Broili, F. (1907). Ein neuer *Ichthyosaurus* aus der norddeutschen Kreide. *Palaeontographica*, 54(2–3), 139–162.

Cadena, E. A. (2015). The first South American sandownid turtle from the Lower Cretaceous of Colombia. *PeerJ,* 3, e1431. https://doi.org/10.7717/peerj.1431

Cadena, E. A., & Parham, J. F. (2015). Oldest known marine turtle? A new protostegid from the Lower Cretaceous of Colombia. *PaleoBios,* 32. https://doi.org/10.5070/p9321028615

Cadena, E. A., Parra-Ruge, M. L., Parra-Ruge, J. de D., & Padilla-Bernal, S. (2019). A gravid fossil turtle from the Early Cretaceous reveals a different egg development strategy to that of extant marine turtles. *Palaeontology,* 62(4), 533-545. https://doi.org/10.1111/pala.12413

Campos, L., Fernández, M. S., & Herrera, Y. (2019). A new ichthyosaur from the Late Jurassic of north-west Patagonia (Argentina) and its significance for the evolution of the narial complex of the ophthalmosaurids. *Zoological Journal of the Linnean Society,* 188(1), 180-201. https://doi.org/10.1093/zoolinnean/zlz095

Campos, L., Fernández, M. S., Herrera, Y., & Garrido, A. (2021). Morphological disparity in the evolution of the ophthalmosaurid forefin: New clues from the Upper Jurassic of Argentina. *Papers in Palaeontology,* 7(4), 1995-2020. https://doi.org/10.1002/spp2.1374

Carballido, J. L., Pol, D., Parra Ruge, M. L., Padilla Bernal, S., Páramo-Fonseca, M. E., & Etayo-Serna, F. (2015). A new Early Cretaceous brachiosaurid (Dinosauria, Neosauropoda) from northwestern Gondwana (Villa de Leiva, Colombia). *Journal of Vertebrate Paleontology,* 35(5), e980505. https://doi.org/10.1080/02724634.2015.980505

Carrillo-Briceño, J. D., Parra, J. D., & Luque, J. (2019). A new lamniform shark *Protolamna ricaurtei* sp. nov. from the Lower Cretaceous of Colombia. *Cretaceous Research,* 95, 336-340. https://doi.org/10.1016/J.CRETRES.2018.12.007

Carter, J. (1846). Notice of the jaws of an *Ichthyosaurus* from the chalk in the neighbourhood of Cambridge. *Reports of the British Association for the Advancement of Science,* 1-60.

Cortés, D., Larsson, H. C. E., Maxwell, E. E., Parra Ruge, M. L., Patarroyo, P., & Wilson, J. A. (2019). An Early Cretaceous Teleosauroid (Crocodylomorpha: Thalattosuchia) from Colombia. *Ameghiniana,* 56(5), 365-379. https://doi.org/10.5710/AMGH.26.09.2019.3269

Cortés, D., Maxwell, E. E., & Larsson, H. C. E. (2021). Re-appearance of hypercarnivore ichthyosaurs in the Cretaceous with differentiated dentition: Revision of '*Platypterygius*' *sachicarum* (Reptilia: Ichthyosauria, Ophthalmosauridae) from Colombia. *Journal of Systematic Palaeontology,* 19(14), 969-1002. https://doi.org/10.1080/14772019.2021.1989507

Cortés, D. & Páramo-Fonseca, M. E. (2018). Restos apendiculares de un ictiosaurio oftalmosáurido del Barremiano inferior de Villa de Leiva, Colombia. *Boletín de Geología,* 40(1), 15-30. https://doi.org/10.18273/REVBOL.V40N1-2018001

Delsett, L. L., Roberts, A. J., Druckenmiller, P. S., & Hurum, J. H. (2019). Osteology and phylogeny of Late Jurassic ichthyosaurs from the Slottsmøya Member Lagerstätte (Spitsbergen, Svalbard). *Acta Palaeontologica Polonica,* 717-743. https://doi.org/10.4202/app.00571.2018

Druckenmiller, P. S., Hurum, J. H., Knutsen, E., & Nakrem, H. (2012). Two new ophthalmosaurids (Reptilia: Ichthyosauria) from the Agardhfjellet Formation (Upper Jurassic: Volgian/Tithonian), Svalbard, Norway. *Norsk Geologisk Tidsskrift,* 92, 311-339.

Druckenmiller, P. S., & Maxwell, E. E. (2010). A new Lower Cretaceous (lower Albian) ichthyosaur genus from the Clearwater Formation, Alberta, Canada. *Canadian Journal of Earth Sciences,* 47(8), 1037-1053. https://doi.org/10.1139/E10-028

Edmund, A. G. (1960). Tooth replacement phenomena in the lower vertebrates. *Life Sciences Contributions, Royal Ontario Museum,* 52, 1-190. https://doi.org/10.5962/bhl.title.52196

Efimov, V. M. (1997). A New Genus of Ichthyosaurs from the Late Cretaceous of the Ulyanovsk Volga Region. *Paleontologicheskii Zhurnal,* 4, 77-82.

Efimov V. M. (1998). An ichthyosaur, *Otschevia pseudoscythica* gen. et sp. nov. from the Upper Jurassic strata of the Ulyanovsk region. *Paleontological Journal,* 32(2), 187-191.

Efimov, V. M. (1999). A new family of ichthyosaurs, the Undorosauridae fam. nov. from the Volgian stage of the European part of Russia. *Paleontological Journal,* 33, 174-181.

Etayo-Serna, F. (1965). Sinopsis estratigráfica de la región de Villa de Leiva y zonas próximas. *Boletín de Geología,* 21, 19-32. https://revistas.uis.edu.co/index.php/revistaboletindegeologia/article/view/7041

Etayo-Serna, F. (1968a). El Sistema Cretáceo en la región de Villa de Leiva y zonas próximas. *Geología Colombiana,* 5, 5-74. https://revistas.unal.edu.co/index.php/geocol/article/view/30374

Etayo-Serna, F. (1968b). Apuntaciones acerca de algunas amonitas interesantes del Hauteriviano y del barremiano de la region de Villa de Leiva (Boyacá, Colombia, S.A.). *Boletín de Geología,* 24, 51-70. https://revistas.uis.edu.co/index.php/revistaboletindegeologia/article/view/6574

Etayo-Serna, F. (1979). *Zonation of the Cretaceous of Central Colombia by Ammonites.* Publicaciones Geológicas Especiales Del Ingeominas, 186 pp.

Farris, J. S. (1989). The Retention Index and the Rescaled Consistency Index. *Cladistics,* 5(4), 417-419. https://doi.org/10.1111/J.1096-0031.1989.TB00573.X

Fernández, M. S. (1997). A new ichthyosaur from the Tithonian (Late Jurassic) of the Neuquén basin, northwestern Patagonia, Argentina. *Journal of Paleontology,* 71(3), 479-484. Scopus. https://doi.org/10.1017/S0022336000039494

Fernández, M. S. (2007). Redescription and Phylogenetic position of *Caypullisaurus* (Ichthyosauria: Ophthalmosauridae). *Journal of Paleontology,* 81(2), 368-375. https://doi.org/10.1666/0022-3360(2007)81[368:RAPPOC]2.0.CO;2

Fernández, M. S., & Aguirre-Urreta, M. B. (2005). Revision of *Platypterygius hauthali* von Huene, 1927 (Ichthyosauria: Ophthalmosauridae) from the Early Cretaceous of Patagonia, Argentina. *Journal of Vertebrate Paleontology,* 25(3), 583-587. https://doi.org/10.1671/0272-4634(2005)025[0583:ROPHVH]2.0.CO;2

Fernández, M. S., Archuby, F., Talevi, M., & Ebner, R. (2005). Ichthyosaurian eyes: Paleobiological information content in the sclerotic ring of *Caypullisaurus* (Ichthyosauria, Ophthalmosauria). *Journal of Vertebrate Paleontology,* 25(2), 330-337. https://doi.org/10.1671/0272-4634(2005)025[0330:IEPICI]2.0.CO;2

Fernández, M. S., Campos, L., Maxwell, E. E., & Garrido, A. C. (2021). *Catutosaurus gaspariniae*, gen. et sp. nov. (Ichthyosauria, Thunnosauria) of the Upper Jurassic of Patagonia and the evolution of the ophthalmosaurids. *Journal of Vertebrate Paleontology,* 41(1), e1922427. https://doi.org/10.1080/02724634.2021.1922427

Fischer, V. (2012). New data on the ichthyosaur *Platypterygius hercynicus* and its implications for the validity of the genus. *Acta Palaeontologica Polonica,* 57(1), 123-134. https://doi.org/10.4202/APP.2011.0007

Fischer, V. (2016). Taxonomy of *Platypterygius campylodon* and the diversity of the last ichthyosaurs. *PeerJ,* 4, e2604. https://doi.org/10.7717/PEERJ.2604/SUPP-2

Fischer, V., Appleby, R. M., Naish, D., Liston, J., Riding, J. B., Brindley, S., & Godefroit, P. (2013). A basal thunnosaurian from Iraq reveals disparate phylogenetic origins for Cretaceous ichthyosaurs. *Biology Letters,* 9(4). https://doi.org/10.1098/RSBL.2013.0021

Fischer, V., Bardet, N., Guiomar, M. & Godefroit, P. (2014a). High Diversity in Cretaceous Ichthyosaurs from Europe Prior to Their Extinction. *PLOS ONE,* 9(1), e84709. https://doi.org/10.1371/journal.pone.0084709

Fischer, V., Arkhangelsky, M. S., Uspensky, G. N., Stenshin, I. M., & Godefroit, P. (2014b). A new Lower Cretaceous ichthyosaur from Russia reveals skull shape conservatism within Ophthalmosaurinae. *Geological Magazine,* 151(1), 60-70. https://doi.org/10.1017/S0016756812000994

Fischer, V., Arkhangelsky, M. S., Naish, D., Stenshin, I. M., Uspensky, G. N., & Godefroit, P. (2014c). *Simbirskiasaurus* and *Pervushovisaurus* reassessed: Implications for the taxonomy and cranial osteology of Cretaceous platypterygiine ichthyosaurs. *Zoological Journal of the Linnean Society,* 171(4), 822-841. https://doi.org/10.1111/ZOJ.12158/SUPPINFO

Fischer, V., Bardet, N., Benson, R. B. J., Arkhangelsky, M. S., & Friedman, M. (2016). Extinction of fish-shaped marine reptiles associated with reduced evolutionary rates and global environmental volatility. *Nature Communications,* 7(1), 1-11. https://doi.org/10.1038/ncomms10825

Fischer, V., Maisch, M. W., Naish, D., Kosma, R., Liston, J., Joger, U., Krüger, F. J., Pérez, J. P., Tainsh, J., & Appleby, R. M. (2012). New Ophthalmosaurid Ichthyosaurs from the European Lower Cretaceous Demonstrate Extensive Ichthyosaur Survival across the Jurassic–Cretaceous Boundary. *PLOS ONE,* 7(1), e29234. https://doi.org/10.1371/JOURNAL.PONE.0029234

Fischer, V., Masure, E., Arkhangelsky, M. S., & Godefroit, P. (2011). A new Barremian (Early Cretaceous) ichthyosaur from western Russia. *Journal of Vertebrate Paleontology,* 31(5), 1010-1025. https://doi.org/10.1080/02724634.2011.595464

Forero, H., & Sarmiento, L. (1985). La facies evaporítica de la Formación Paja en la región de Villa de Leiva. In: Etayo-Serna, F., & Laverde, F. (Editors). *Proyecto Cretácico*. Publicaciones geológicas especiales de Ingeominas, Bogotá, Colombia, 1-16.

Goloboff, P. A. & Morales, M. E. (2023). TNT version 1.6, with a graphical interface for MacOS and Linux, including new routines in parallel. *Cladistics,* 39(2), 144-153. https://doi.org/10.1111/CLA.12524

Gómez-Pérez, M., & Noè, L. F. (2017). Cranial anatomy of a new pliosaurid *Acostasaurus pavachoquensis* from the Lower Cretaceous of Colombia, South America. *Palaeontographica Abteilung A,* 310(1-2), 5-42. https://doi.org/10.1127/PALA/2017/0068

Hoedemaeker, P. J. (2004). On the Barremian—Lower Albian stratigraphy of Colombia. *Scripta Geologica,* 128, 3-15.

Huene, F. (1922). Die Ichthyosaurier des Lias und ihre Zusammenhänge. *Verlag von Gebrüder Borntraeger,* 1, 1-114.

Huene, F. (1927). Beitrag zur Kenntnis mariner mesozoischer Wirbeltiere in Argentinien. *Centralblatt Für Mineralogie, Geologie Und Paläontologie, B*, 22-29.

Huertas, G. (1970). Sertum florulae fossilis Villae de Leiva II. *Caldasia,* 10(50), 595-602. https://revistas.unal.edu.co/index.php/cal/article/view/34315

Jack, R. L., & Etheridge, R. (1892). *The geology and palaeontology of Queensland and New Guinea, with sixty-eight plates and a geological map of Queensland (Vol. 1).* James Charles Beal, Government Printer, Brisbane, Australia, 804 pp. https://doi.org/10.5962/bhl.title.131227

Jacobs, M. L., & Martill, D. M. (2020). A new ophthalmosaurid ichthyosaur from the Upper Jurassic (Early Tithonian) Kimmeridge Clay of Dorset, UK, with implications for Late Jurassic ichthyosaur diversity. *PLOS ONE,* 15(12), e0241700. https://doi.org/10.1371/JOURNAL.PONE.0241700

Ji, C., Jiang, D. Y., Motani, R., Rieppel, O., Hao, W. C., & Sun, Z. Y. (2016). Phylogeny of the Ichthyopterygia incorporating recent discoveries from South China. *Journal of Vertebrate Paleontology,* 36(1), e1025956. https://doi.org/10.1080/02724634.2015.1025956

Kear, B. P. (2005). Cranial morphology of *Platypterygius longmani* Wade, 1990 (Reptilia: Ichthyosauria) from the Lower Cretaceous of Australia. *Zoological Journal of the Linnean Society*, 145(4), 583-622. https://doi.org/10.1111/j.1096-3642.2005.00199.x

Kear, B. P., & Zammit, M. (2014). In utero foetal remains of the Cretaceous ichthyosaurian *Platypterygius*: Ontogenetic implications for character state efficacy. *Geological Magazine,* 151(1), 71-86. https://doi.org/10.1017/S0016756813000113

Kiprijanoff, W. (1881). Studien über die fossilen reptilien Russlands. Gattung *Ichthyosaurus* könig aus dem Severischen Sandstein oder Osteolith der Kreide-Gruppe. *Mémoires de L'Académie Impériale Des Sciences de St. Pétersbourg,* 28(7), 1-103.

Kolb, C., & Sander, P. M. (2009). Redescription of the ichthyosaur *Platypterygius hercynicus* (Kuhn 1946) from the Lower Cretaceous of Salzgitter (Lower Saxony, Germany). *Palaeontographica Abteilung A,* 288(4-6), 151-192. https://doi.org/10.1127/PALA/288/2009/151

Kuhn, O. (1946). Ein skelett von *Ichthyosaurus hercynicus* n. sp. aus dem Aptien von Gitter. *Berichte Der Naturforschenden Gesellschaft Bamberg,* 29, 69-82.

Longman, H. (1922). An ichthyosaurian skull from Queensland. *Memoirs of the Queensland Museum,* 7, 246-256.

Lydekker, R. (1888). VI.—Note on the Classification of the Ichthyopterygia (with a Notice of Two New Species). *Geological Magazine,* 5(7), 309-314. https://doi.org/10.1017/S0016756800181968

Maddison, W., & Maddison, D. (2018). *MESQUITE: a modular system for evolutionary analysis. Version 3.51.* http://www.mesquiteproject.org

Maisch, M., & Matzke, A. (2000). The Ichthyosauria. *Stuttgarter Beiträge Zur Naturkunde Serie B,* 298, 1–159.

Manolov, J. R. (1962). New ammonites from the Barremian of north Bulgaria. *Palaeontology,* 5(3), 527-539.

Maxwell, E. E. (2010). Generic reassignment of an ichthyosaur from the Queen Elizabeth Islands, Northwest Territories, Canada. *Journal of Vertebrate Paleontology,* 30(2), 403-415. https://doi.org/10.1080/02724631003617944

Maxwell, E. E., & Caldwell, M. W. (2006a). A new genus of Ichthyosaur from the Lower Cretaceous of Western Canada. *Palaeontology,* 49(5), 1043-1052. https://doi.org/10.1111/J.1475-4983.2006.00589.X

Maxwell, E. E., & Caldwell, M. W. (2006b). Evidence for a second species of the ichthyosaur *Platypterygius* in North America: A new record from the Loon River Formation (Lower Cretaceous) of northwestern Canada. *Canadian Journal of Earth Sciences,* 43(9), 1291-1295. https://doi.org/10.1139/e06-029

Maxwell, E. E., Caldwell, M. W., & Lamoureux, D. O. (2011). Tooth histology in the Cretaceous ichthyosaur *Platypterygius australis*, and its significance for the conservation and divergence of mineralized tooth tissues in amniotes. *Journal of Morphology,* 272(2), 129-135. https://doi.org/10.1002/jmor.10898

Maxwell, E. E., Cortés, D., Patarroyo, P., & Ruge, M. L. P. (2019). A new specimen of *Platypterygius sachicarum* (Reptilia, Ichthyosauria) from the Early Cretaceous of Colombia and its phylogenetic implications. *Journal of Vertebrate Paleontology,* 39(1). https://doi.org/10.1080/02724634.2019.1577875

Maxwell, E. E., Dick, D., Padilla, S., & Parra, M. L. (2016). A new ophthalmosaurid ichthyosaur from the Early Cretaceous of Colombia. *Papers in Palaeontology,* 2(1), 59-70. https://doi.org/10.1002/SPP2.1030

Maxwell, E. E. & Kear, B. P. (2010). Postcranial anatomy of *Platypterygius americanus* (Reptilia: Ichthyosauria) from the Cretaceous of Wyoming. *Journal of Vertebrate Paleontology,* 30(4), 1059-1068. https://doi.org/10.1080/02724634.2010.483546

Mazin, J. M. (1983). L'implantation dentaire chez les Ichthyopterygia (Reptilia). *Neues Jahrbuch für Geologie und Paläontologie - Monatshefte,* 7, 406-418. https://doi.org/10.1127/njgpm/1983/1983/406

McDowell, S. B. (1967). The Extracolumella and Tympanic Cavity of the "Earless" Monitor Lizard, Lanthanotus borneensis. *Copeia,* 1967(1), 154-159. https://doi.org/10.2307/1442189

McGowan, C. (1972). The systematics of Cretaceous ichthyosaurs with particular reference to the material from North America. *Rocky Mountain Geology,* 11(1), 9-29.

McGowan, C. (1997). The taxonomic status of the Late Jurassic Ichthyosaur *Grendelius mordax*: A preliminary report. *Journal of Vertebrate Paleontology,* 17(2), 428-430. https://doi.org/10.1080/02724634.1997.10010986

McGowan, C., & Motani, R. (2003). *Ichthyopterygia.* Dr. Friedrich Pfeil. Munich, Germany, 173 pp.

M'Coy, F. (1867). L.—On the occurrence of Ichthyosaurus and Plesiosaurus in Australia. *Annals and Magazine of Natural History,* 19(113), 355-356. https://doi.org/10.1080/00222936708562678

Moon, B. C. (2019). A new phylogeny of ichthyosaurs (Reptilia: Diapsida). *Journal of Systematic Palaeontology,* 17(2), 129-155. https://doi.org/10.1080/14772019.2017.1394922

Moon, B. C. & Kirton, A. M. (2016). Ichthyosaurs of the British Middle and Upper Jurassic Part 1, *Ophthalmosaurus. Monographs of the Palaeontographical Society,* 170(647), 1-84. https://doi.org/10.1080/02693445.2016.11963958

Nace, R. L. (1939). A new ichthyosaur from the Upper Cretaceous Mowry Formation of Wyoming. *American Journal of Science,* 237(9), 673-686. https://doi.org/10.2475/ajs.237.9.673

Noè, L. F., & Gómez–Pérez, M. (2020). Plesiosaurs, Palaeoenvironments, and the Paja Formation Lagerstätte of Central Colombia: An Overview. In: Gómez, J., & Pinilla–Pachon, A. O. (Editors). *The Geology of Colombia, Volume 2 Mesozoic.* Publicaciones Geológicas Especiales 36, Servicio Geológico Colombiano, Bogotá, Colombia, 441-483. https://doi.org/10.32685/pub.esp.36.2019.13

Noè, L. F., & Gómez-Pérez, M. (2022). Giant pliosaurids (Sauropterygia; Plesiosauria) from the Lower Cretaceous peri-Gondwanan seas of Colombia and Australia. *Cretaceous Research,* 132, 105122. https://doi.org/10.1016/J.CRETRES.2021.105122

Ochev, V. G., & Efimov, V. M. (1985). A new genus of Ichthyosaur from the Ul'Yanovsk area of the Povolzh'ye Region. *Paleontological Journal,* 4, 87-91.

Padilla, C. B., Páramo-Fonseca, M. E., Noè, L. F., Gómez Pérez, M., & Luz Parra, M. (2010). Acid Preparation of Large Vertebrate Specimens. *Geological Curator,* 9(3), 213-220. https://doi.org/10.55468/GC231

Palci, A., Caldwell, M. W., Hutchinson, M. N., Konishi, T., & Lee, M. S. Y. (2020). The morphological diversity of the quadrate bone in squamate reptiles as revealed by high-resolution computed tomography and geometric morphometrics. *Journal of Anatomy,* 236(2), 210-227. https://doi.org/10.1111/JOA.13102

Paparella, I., Maxwell, E. E., Cipriani, A., Roncacè, S., & Caldwell, M. W. (2016). The first ophthalmosaurid ichthyosaur from the Upper Jurassic of the Umbrian–Marchean Apennines (Marche, Central Italy). *Geological Magazine,* 154(4), 837-858. https://doi.org/10.1017/S0016756816000455

Páramo, M. E. (1997). *Platypterygius sachicarum* (Reptilia, Ichthyosauria) nueva especie del Cretácico de Colombia. *Revista Ingeominas,* 6, 1-12.

Páramo-Fonseca, M. E. (2015). Estado Actual del Conocimiento de los Reptiles Marinos Cretácicos de Colombia. *Publicación Electrónica de La Asociación Paleontológica Argentina,* 40-57. https://doi.org/10.5710/peapa.12.06.2015.98

Páramo-Fonseca, M. E., Benavides-Cabra, C. D., & Gutiérrez, I. E. (2018). A new large Pliosaurid from the Barremian (Lower Cretaceous) of Sáchica, Boyacá, Colombia. *Earth Sciences Research Journal,* 22(4), 223-238. https://doi.org/10.15446/esrj.v22n4.69916

Páramo-Fonseca, M. E., Benavides-Cabra, C. D., & Gutiérrez, I. E. (2019a). A new specimen of *Stenorhynchosaurus munozi* Páramo-Fonseca et al., 2016 (Plesiosauria, Pliosauridae), from the Barremian of Colombia: New morphological features and ontogenetic implications. *Journal of Vertebrate Paleontology,* 39(4). https://doi.org/10.1080/02724634.2019.1663426

Páramo-Fonseca, M. E., García-Guerrero, J., Benavides-Cabra, C. D., Padilla-Bernal, S., & Castañeda-Gómez, A. J. (2021). A benchmark specimen of *Muiscasaurus catheti* from the upper Aptian of Villa de Leiva, Colombia: New anatomical features and phylogenetic implications. *Cretaceous Research,* 119, 104685. https://doi.org/10.1016/J.CRETRES.2020.104685

Páramo-Fonseca, M. E., Gómez-Pérez, M., Noé, L. F., & Etayo-Serna, F. (2016). *Stenorhynchosaurus munozi*, gen. et sp. nov. un pliosaurido nuevo del Barremiano superior (Cretácico Inferior) de Villa de Leiva, Colombia, Suramérica. *Revista de La Academia Colombiana de Ciencias Exactas, Físicas y Naturales,* 40(154), 84-103. https://doi.org/10.18257/RACCEFYN.239

Páramo-Fonseca, M. E., O'Gorman, J. P., Gasparini, Z., Padilla, S., & Parra-Ruge, M. L. (2019b). A new late Aptian elasmosaurid from the Paja Formation, Villa de Leiva, Colombia. *Cretaceous Research,* 99, 30-40. https://doi.org/10.1016/J.CRETRES.2019.02.010

Patarroyo, P. (2000). Distribución de Amonitas del Barremiano de la Formación Paja en el Sector de Villa de Leyva (Boyacá, Colombia). Bioestratigrafía. *Geología Colombiana,* 25, 149-162. https://revistas.unal.edu.co/index.php/geocol/article/view/31539

Patarroyo, P. (2004). The development of the Barremian Pulchelliidae family ammonites from central Colombia (South America). *Revue de Paléobiologie,* 23, 1-65.

Patarroyo, P. (2009). Amonitas de un nivel de alta energía del Barremiano inferior en la Formación Paja de los sectores de Villa de Leyva (Boyacá) y de Vélez (Santander). *Boletín de Geología,* 31(2), 15-21. https://revistas.uis.edu.co/index.php/revistaboletindegeologia/article/view/344

Patarroyo, P. (2020). Barremian Deposits of Colombia: A Special Emphasis on Marine Successions. In: Gómez, J., & Pinilla–Pachon, A. O. (Editors). *The Geology of Colombia, Volume 2 Mesozoic.* Publicaciones Geológicas Especiales 36, Servicio Geológico Colombiano, Bogotá, Colombia, 403-439. https://doi.org/10.32685/pub.esp.36.2019.12

Pol, D., & Escapa, I. H. (2009). Unstable taxa in cladistic analysis: Identification and the assessment of relevant characters. *Cladistics,* 25(5), 515-527. https://doi.org/10.1111/J.1096-0031.2009.00258.X

R Core Team. (2022). *R: A Language and Environment for Statistical Computing.* R Foundation for Statistical Computing, Vienna, Austria, https://www.R-project.org/ (last accessed November 2023).

Romer, A. S. (1968). An ichthyosaur skull from the Cretaceous of Wyoming. *Rocky Mountain Geology,* 7(1), 27-41.

Schultze, H. P., & Stöhr, D. (1996). *Vinctifer* (Pisces, Aspidorhynchidae) aus der Unterkreide (oberes Aptium) von Kolumbien. *Neues Jahrbuch Fur Geologie Und Palaontologie - Abhandlungen,* 199(3), 395-415. https://doi.org/10.1127/NJGPA/199/1996/395

Seeley, H. G. (1874). On the pectoral arch and fore limb of *Ophthalmosaurus*, a new ichthyosaurian genus from the Oxford Clay. *Quarterly Journal of the Geological Society of London,* 30, 696-707.

Van Waveren, I. M., van Konijnenburg - van Cittert, J., van der Burgh, J., & Dilcher, D. L. (2002). Macrofloral remains from the Lower Cretaceous of the Leiva region (Colombia). *Scripta Geologica,* 123, 1-39.

Wade, M. (1984). *Platypterygius australis*, an Australian Cretaceous ichthyosaur. *Lethaia,* 17(2), 99-113. https://doi.org/10.1111/j.1502-3931.1984.tb01713.x

Wade, M. (1990). A review of the Australian Cretaceous longipinnate ichthyosaur *Platypterygius* (Ichthyosauria, Ichthyopterygia). *Memoirs of the Queensland Museum,* 28(1), 115-137.

Zammit, M. (2010). A review of Australasian ichthyosaurs. *Alcheringa: An Australasian Journal of Palaeontology,* 34(3), 281-292. https://doi.org/10.1080/03115511003663939

Zammit, M. (2011). The Australian Cretaceous ichthyosaur *Platypterygius australis*: Understanding its taxonomy, morphology, and palaeobiology. [Ph.D. Dissertation, University of Adelaide], Adelaide, South Australia. https://digital.library.adelaide.edu.au/dspace/handle/2440/70731

Zammit, M., Norris, R. M., & Kear, B. P. (2010). The Australian Cretaceous ichthyosaur *Platypterygius australis*: A description and review of postcranial remains. *Journal of Vertebrate Paleontology,* 30(6), 1726-1735. https://doi.org/10.1080/02724634.2010.521930

Zverkov, N. G. (2022). A Problem of Naming of the Families of Late Jurassic and Cretaceous Ichthyosaurs. *Paleontological Journal,* 56(4), 463-470. https://doi.org/10.1134/S0031030122040141

Zverkov, N. G., Arkhangelsky, M. S., & Stenshin, I. M. (2022). New Data on Late Jurassic Ichthyosaurs of the Genus *Grendelius* from European Russia. *Paleontological Journal,* 56(11), 1459-1481. https://doi.org/10.1134/S003103012211020X

Zverkov, N. G., & Efimov, V. M. (2019). Revision of *Undorosaurus*, a mysterious Late Jurassic ichthyosaur of the Boreal Realm. *Journal of Systematic Palaeontology,* 17(14), 1183-1213. https://doi.org/10.1080/14772019.2018.1515793

Zverkov, N. G., & Grigoriev, D. V. (2020). An unrevealed lineage of platypterygiines (Ichthyosauria) with peculiar forefin structure and semiglobal distribution in the mid-Cretaceous (Albian–Cenomanian). *Cretaceous Research,* 115, 104550. https://doi.org/10.1016/j.cretres.2020.104550

Zverkov, N. G., & Jacobs, M. L. (2021). Revision of *Nannopterygius* (Ichthyosauria: Ophthalmosauridae): Reappraisal of the 'inaccessible' holotype resolves a taxonomic tangle and reveals an obscure ophthalmosaurid lineage with a wide distribution. *Zoological Journal of the Linnean Society,* 191(1), 228-275. https://doi.org/10.1093/ZOOLINNEAN/ZLAA028

Zverkov, N. G., & Prilepskaya, N. E. (2019). A prevalence of *Arthropterygius* (Ichthyosauria: Ophthalmosauridae) in the Late Jurassic-earliest Cretaceous of the boreal realm. *PeerJ,* 2019(4), e6799. https://doi.org/10.7717/PEERJ.6799/SUPP-2